Quantum Mechanical Methods for Enzyme Kinetics

Jiali Gao and Donald G. Truhlar

Department of Chemistry and Supercomputer Institute, University of Minnesota,
207 Pleasant Street S.E., Minneapolis, Minnesota 55455-0431;
e-mail: gao@chem.umn.edu; truhlar@umn.edu

Key Words   catalysis, dynamics, free energy, potential of mean force, QM/MM, rate constant, tunneling, variational transition state theory

■ **Abstract**   This review discusses methods for the incorporation of quantum mechanical effects into enzyme kinetics simulations in which the enzyme is an explicit part of the model. We emphasize three aspects: (*a*) use of quantum mechanical electronic structure methods such as molecular orbital theory and density functional theory, usually in conjunction with molecular mechanics; (*b*) treating vibrational motions quantum mechanically, either in an instantaneous harmonic approximation, or by path integrals, or by a three-dimensional wave function coupled to classical nuclear motion; (*c*) incorporation of multidimensional tunneling approximations into reaction rate calculations.

INTRODUCTION

The past few years have seen significant progress on the accurate molecular modeling of enzyme reactions. This review summarizes recent progress on incorporating quantum mechanical effects into such modeling.

Almost all enzyme reactions can be well described by the Born-Oppenheimer approximation, in which the sum of the electronic energy and the nuclear repulsion provides a potential energy function, or potential energy surface (PES), governing the interatomic motions. Therefore the molecular modeling problem breaks into two parts: the PES and the dynamics. After a brief overview in the next section, we consider these in turn in the following section. The final section surveys applications.

THEORETICAL FRAMEWORK OF ENZYME KINETICS

The key to elucidating the mechanism of enzymatic reactions is an understanding of the specific interactions between the substrate and its enzyme environment and their effect on the reaction rate. Although our emphasis in this review is quantum mechanical effects in enzymology, we begin by considering classical mechanical

rate theory and then proceed to discuss the way in which quantum mechanical contributions can be included. The starting point of our discussion is transition state theory (TST) (1–12), which is based on a hypersurface (the transition state) that divides reactants from products in phase space. TST can be derived based on two fundamental assumptions: (*a*) Reactant states are in local equilibrium along a progress coordinate, which is the reaction coordinate, and (*b*) trajectories that cross the transition state hypersurface do not recross it before becoming thermalized on the reactant or product side (7, 13). When these assumptions are satisfied, the TST rate constant, which is the local equilibrium one-way flux coefficient for crossing the hypersurface in the direction of products, is equal to the net reactive flux coefficient, which is the observed rate constant. Because it neglects recrossing, the classical TST rate gives an upper limit to the true classical reaction rate for the case in which reactant states are in equilibrium with each other even though they are not in equilibrium with the product. The dynamic recrossing can be taken into account by a transmission coefficient (4, 8, 14–16). Thus, the exact classical rate constant at temperature T can be written as

$$k(T) = \gamma(T)\frac{1}{\beta h} \exp[-\beta \Delta G^{\neq}(T)], \qquad 1.$$

where $\gamma(T)$ is the transmission coefficient, $\beta = 1/k_B T$, k_B is Boltzmann's constant, h is Planck's constant, and $\Delta G^{\neq}(T)$ is the molar free energy of activation. Note that both $\Delta G^{\neq}(T)$ and $\gamma(T)$ depend on the choice of the transition state hypersurface, and thus they have a complementary nature. A "better" transition state hypersurface leads to a higher $\Delta G^{\neq}(T)$ and a larger $\gamma(T)$, at least in classical mechanics. The theory may be applied to gas-phase reactions (1–12) and to reactions in condensed phases including enzymes (8, 10–13, 17–21). Experience has shown that TST provides accurate estimates of rate constant, provided that one chooses the location of the dividing surface along the reaction coordinate to minimize the calculated rate constant; this is called variational TST (VTST) (5) to emphasize the variation or TST for simplicity. For the purposes of this review, TST is especially important because it provides a clear route to the incorporation of quantum effects (9, 11, 22), which we consider below.

Equation 1 shows that there are two critical quantities to be evaluated: the equilibrium free energy of activation $\Delta G^{\neq}(T)$ and the dynamical transmission coefficient $\gamma(T)$. In many cases the more important of these quantities is the former because the rate constant depends exponentially on the free energy of activation. Thus, it is not surprising that major efforts have been devoted to developing methods for the accurate description of PESs that allow one to estimate free energies of activation. In classical mechanics one can always, in principle, find a hypersurface for gas phase reaction such that there are no recrossings, and hence $\gamma(T)$ has a value of unity. However, such a hypersurface may be very intricate, and finding it may be equivalent to solving the full dynamic problem.

Let z be the reaction coordinate or progress variable. For multidimensional condensed-phase systems such as reactions in enzymes, a one-dimensional

optimization of the transition state location along z is usually carried out. In such cases it is not always clear how best to choose the reaction coordinate. Most work uses a simple function of valence coordinates (e.g., making and breaking bond distances) (23, 24), whereas other studies employ a collective bath coordinate, as in Marcus theory (25–28). In practice, a good choice of the reaction coordinate, z, plus optimization of the location of the transition state hypersurface along z and sometimes of its orientation relative to z is expected to result in a transmission coefficient with a value close to 1, making it quantitatively unimportant. On the other hand, a poor choice of the reaction coordinate or the transition state will require more effort in computing $\gamma(T)$, which might have a significantly reduced value. In VTST one optimizes the transition state hypersurface to minimize the need for a recrossing correction (1, 3, 5, 6, 8–12, 29, 30).

The equilibrium assumption is normally expected to be well satisfied except for very fast reactions (31). The word "equilibrium" is sometimes used in a second way to describe TST. If a set of coordinates **x** are not involved in the definition of the reaction coordinate z, the TST one-way flux expression can be derived by assuming that coordinates **x** are equilibrated instantaneously with respect to motion along z, although TST does not require this. Nevertheless, in this sense the statement that coordinates are not in equilibrium is the same as saying that they should be included in the reaction coordinate by including them in the definition of the transition state. Thus, an effect that is a nonequilibrium contribution for one choice of transition state hypersurface may be an equilibrium contribution for another. If mode m of the bath is not in equilibrium with motion along the reaction coordinate, it exerts a frictional effect on it. In such a case the calculation can be improved in two ways: (*a*) including mode m in the definition of the reaction coordinate to optimize the definition of the transition state hypersurface (because the reaction coordinate is defined as motion orthogonal to that hypersurface) or (*b*) including these "nonequilibrium" or frictional effects in a transmission coefficient that is less than unity to account for recrossing.

Note that the transition state is not a single structure. It is an ensemble of structures, and the free energy of activation is related to the potential of mean force (PMF), $W(T, z)$ (8, 11, 15, 24, 32–34), that is obtained by averaging over protein, substrate, and solvent configurations along z. Thus, in classical mechanics, denoted by CM,

$$\Delta G^{\neq}(T) = W_{CM}(T, z^{\neq}) - \left[W_{CM}(T, z_R) + G_{CM}^R(z) \right] + C(T, z), \qquad 2.$$

where z_R and $z^{\neq}$ are values of the reaction coordinate at the reactant state and at the transition state, $G_{CM}^R(z)$ corresponds to the free energy of the mode in the reactant (R) state that correlates with the progress coordinate z, and $C(T, z)$ is a small correction term that is due to the Jacobian of the transformation from a locally rectilinear reaction coordinate to the curvilinear reaction coordinate z.

The CM potential of mean force is defined by

$$W_{CM}(T, z) = -RT \ln \rho_{CM}(T, z) + W_{CM}^o, \qquad 3.$$

where $\rho_{CM}(T, z)$ represents the classical mechanical probability density as a function of z, which can be evaluated by carrying out molecular dynamics or Monte Carlo simulations using umbrella sampling (35) or free energy perturbation techniques (36).

Quantum mechanics enters the computation of the PMF and free energy of activation in two major ways. First, the electronic structure of the atoms that are involved in the bond-making and bond-breaking process should be treated quantum mechanically in calculating the PES that governs the motions that determine $W(T, z)$. This is necessary because although traditional molecular mechanics force fields that describe the PES of substrates by a set of parameterized analytical functions have been very successful in optimizing equilibrium structure and give reasonably accurate results for the energy contours for small-amplitude vibrations around such structures (37), they do not have the correct functional form for describing chemical reactions. The reader is referred to key references (38–41) and a recent review (42) for further discussion of molecular mechanics models, the most widely used of which, for enzyme kinetics (including interactions with aqueous solvent), are AMBER, CHARMM, GROMOS, OPLS, and TIP3P. In the section entitled "Potential Energy Surface" we summarize techniques for incorporating electronic structural methods in modeling enzymatic reactions.

The second aspect of quantum mechanics that affects the PMF is the quantum mechanical nature of nuclear motion. In particular, because a reacting system is bound in its transition state as the reaction coordinate is fixed and missing as a degree of freedom, the most important quantum effects on the motions within the transition state hypersurface can be incorporated by the usual methods for bound vibrations (43). As we review in "Potential of Mean Force," it is necessary to incorporate such quantum vibrational effects in evaluation of the free energy of activation. The transmission coefficient, though, may be considered as arising from motions normal to the transition state hypersurface, i.e., dynamical recrossing and tunneling, and from the nonseparability of the reaction coordinate.

The recrossing contribution to the transmission coefficient, $\gamma(T)$, in Equation 1 can be approximated classically by propagating trajectories forward and backward from an ensemble of transition state configurations and counting the number of crossings of the transition state hypersurface. The general formalism for such calculations was first developed systematically by Keck (14) and elaborated by Anderson (4) and others (13, 15, 44). These workers used classical methods to define the transition state ensemble and calculated the transmission coefficient by propagating trajectories forward and backward from phase points in that ensemble for both gas-phase and liquid-phase reactions. This procedure has been extended to an enzyme reaction by Neria & Karplus (21). The next level of sophistication is to select transition state phase points from a semiclassical treatment of the transition state, i.e., from a distribution of transition states with quantized vibrations, but still estimate the recrossing factor from purely classical trajectories (45, 46). Even better, one can both select from a semiclassical distribution of transition states and include quantum effects in the dynamical calculation used to

estimate recrossing. Schenter et al. (47) presented one method for doing this, and we have presented a method that is specifically designed for enzyme reactions to include the effect of quantization transverse to the reaction coordinate on motion along a minimum-energy reaction path (48). Our method leads to the $\Gamma(T)$ factor discussed in "Dynamics and Tunneling." Billeter et al. (49) have presented an alternative approach, also discussed in that section.

The inclusion of the quantum nature of the motion that advances the reaction coordinate, chief among which is tunneling, is the third aspect of quantum mechanical contributions in enzyme kinetics modeling and is also addressed in "Dynamics and Tunneling." A critical aspect is that tunneling requires a multi-dimensional treatment because reaction coordinate motion is not separable (9).

METHODS

From the above discussion, we can see that there are three main ways in which quantum mechanics should be included in enzyme kinetics modeling. First, the electronic structure of the atoms directly involved in the chemical step must be treated quantum mechanically in order to describe the bond-making and bond-breaking processes. Second, the discrete nature of quantum mechanical vibrational energies should be incorporated in the description of nuclear motion for computing the PMF and the transmission coefficient. Finally, consideration of multidimensional tunneling contributions is required in calculating the transmission coefficient, particularly for reactions involving hydrogen (H, H^+, and H^-) transfer. Although quantum mechanical approaches have been used in various ways for studying condensed-phase systems (24, 50), it was only recently that computational studies have fully included all three of these aspects of quantum mechanical effects in calculations including an explicit enzyme environment (48, 51–59). In what follows, we summarize methods that have been developed by our groups and others for including quantum mechanical contributions in enzyme kinetics modeling.

Potential Energy Surface

As explained above, $\Delta G^{\neq}(T)$ results from averaging the PES appropriately over an ensemble of structures, and therefore its accuracy depends on the accuracy of the PES. To compute the PES for macromolecular processes such as enzymatic reactions, it is necessary to use a chemical model that is capable of describing the formation and breaking of chemical bonds and also is suitable for capturing the complexity of the system. A fully quantum mechanical treatment of the entire enzyme system, in principle, satisfies these criteria, and quantum mechanical algorithms designed to involve an effort that scales linearly with system size have been developed and applied to protein systems in energy calculations (60–69). Although this approach has many attractive features, it is very expensive, and this has limited its application to biological problems.

Fortunately, in most enzymatic reactions it is not necessary to treat the electronic structure of the entire enzyme-solvent system quantum mechanically. The most promising approaches for modeling enzymatic reactions are combined quantum mechanical and molecular mechanical (QM/MM) methods, in which a system is divided into a quantum mechanical region and a molecular mechanical region (28, 70–83). The quantum mechanical region typically includes atoms that are directly involved in the chemical step and they are treated explicitly by a quantum mechanical electronic structure method, whereas the molecular mechanical region consists of the rest of the system and is approximated by a molecular mechanical force field. This way of combining quantum mechanics with molecular mechanics was initially developed for gas-phase calculations (84) and was first applied to enzyme systems by Warshel & Levitt (71). A combined QM/MM potential has the advantage of both the computational efficiency offered by molecular mechanics, allowing for free energy simulations of macromolecules, and the computational accuracy provided by quantum mechanics such that the method can be systematically improved (85). The past decade has seen a rapid increase in number and diversity of applications, including reactions in solution (24) and in enzymes (59, 86). The method has been implemented in combination with semiempirical and ab initio molecular orbital theory and with density functional theory (DFT). In fact, combined QM/MM techniques have emerged as the method of choice for modeling enzymatic reactions.
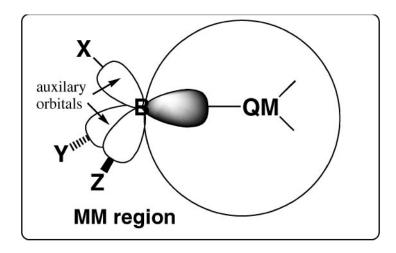
The most popular methods for treating the quantum mechanical subsystem in enzyme reactions have been semiempirical molecular orbital methods (87), such as AM1 (88), PM3 (89), MNDO (90), Hartree-Fock (HF) theory (91), Møller-Plesset perturbation theory (MP2) (91), configuration interaction with single excitations (91), the Becke-Lee-Yang-Parr density functional (92, 93), and the three-parameter hybrid version (B3LYP) (94) of this DFT method. Basis sets have included 3-21G (91) 6-31G* (in which a d shell is added to the 6-31G basis) (91), basis sets designed for use with effective core potentials (95), and plane waves (96).

Combined QM/MM methods have been reviewed in several articles (70, 74, 80, 97, 98) and a full review is not repeated in this article. Here, we focus on the most critical issue in application to enzyme systems, i.e., the treatment of the boundary that separates the quantum mechanical and molecular mechanical regions. Gao et al. identified criteria that they considered to be important for the treatment of a covalent bond at the QM/MM interface (99). First, without introducing extra degrees of freedom, any boundary method should reproduce the correct geometry in comparison with that predicted by the corresponding quantum mechanical calculation on the entire system. Second, the electronic structure, including charge distribution and electrostatic potential, of the full quantum mechanical system should be retained in the quantum mechanical fragment, e.g., the boundary atom should have the same electronegativity as that in the quantum mechanical molecule. Third, the torsional PES about the bond connecting the quantum mechanical region to the molecular mechanical region should be consistent with results from pure quantum mechanical and molecular mechanical calculations.

An early and still widely used scheme is the "link-atom" approach, in which extra, unphysical atoms are added to the quantum mechanical region, one for each bond at the interface to the molecular mechanical region (72, 74). These link atoms, typically hydrogen atoms, are placed at appropriate distances along the bond, and they can be constrained in the direction of the molecular mechanical boundary atom or allowed to freely move. The forces between these link atoms and molecular mechanical atoms are unphysical, so all or some of the forces of the molecular mechanical subsystem on the quantum mechanical subsystem are sometimes omitted. When this is done, the quantum mechanical fragment does not experience the real electrostatic environment of the enzyme active site (100, 101). To circumvent the problem of omitting forces on the link atom, a scaling scheme (scaled-position link-atom method) has been proposed to transfer forces on link atoms to other "physical" atoms (102). Rather than using hydrogen as the link atom, Ostlund (102a) suggested using pseudo-halogen atoms parameterized to mimic the missing valence bond between the quantum mechanical and molecular mechanical subsystems (80), which would also include hyperconjugation interactions owing to the presence of p orbitals. A similar idea has been implemented as a pseudopotential in DFT by Zhang et al. (103).

Other methods dispense with the unphysical link atoms and employ hybrid orbitals. Warshel & Levitt suggested that a hybrid oribital could be used to treat the QM/MM bond, though the approach was not elaborated further (71). Two formalisms that have proved successful for treating the boundary region are strictly localized bond orbitals (104–108) and generalized hybrid orbitals (GHOs) (99, 109). Rivail and coworkers (104–108) called their scheme the local self-consistent field (LSCF) method. In this method the valency of the quantum mechanical boundary atom is saturated by a frozen hybrid orbital with a predetermined density from calculations of a smaller model system. The charge densities of the frozen hybrid orbitals are kept fixed in an SCF calculation of the quantum mechanical system. The LSCF scheme has been developed both for semiempirical (104) and ab initio molecular orbital QM/MM methods (106, 107) and recently it has been extended to DFT (110).

The GHO method, which was initially developed for semiempirical Hamiltonians (99, 109), differs from the LSCF approach in orbital optimization and system partition as illustrated by Figure 1. In the LSCF method the boundary atom is a quantum mechanical atom with a frozen density for the hybrid orbital pointing toward the molecular mechanical fragment, whereas the boundary atom in the GHO scheme is treated as both a quantum mechanical and molecular mechanical atom. The hybridization of the hybrid orbitals on the boundary atom in the GHO method is determined by the molecular geometry and is dynamically varied during the simulation. Furthermore, the charge density of the hybrid orbital that is bonded to the quantum mechanical fragment is optimized self-consistently with all other atomic orbitals in the SCF calculation. An advantage of the GHO method is that it uses fully transferable semiempirical parameters for the boundary atoms in precisely the same way as the standard semiempirical algorithm (99). There are
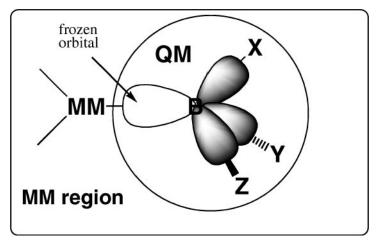
Figure 1   Schematic representation of the local self-consistent field method, (*bottom*) and the generalized hybrid orbital approach, (*top*) for the treatment of a covalent bond across the boundary between the quantum and classical regions. QM, quantum mechanical; MM, molecular mechanical.

no extra degrees of freedom introduced into the system, and all molecular mechanical partial charges are fully retained in SCF calculations. Thus, it provides a better treatment of electrostatic interactions than the link-atom method does. This method has been successfully used to study a number of enzymatic reactions and is being extended to ab initio QM/MM calculations.

Antes & Thiel described a similar approach (111, 112), in which the boundary atom is represented by a hydrogen-like atom with its semiempirical Hamiltonian parameters optimized to reproduce the geometry and energy of a set of model

compounds. Bersuker et al. described a double self-consistent procedure to allow charge transfer (113), as in the GHO method, between the quantum mechanical and molecular mechanical fragments.

The development of satisfactory boundary methods allows combined QM/MM methods to be used effectively in free energy calculations on enzymatic reactions. However, when ab initio or DFT methods are used for the quantum mechanical part, one must use at least a polarized split valence basis set and include electron correlation to achieve the accuracy needed for predicting the enzyme reaction rate. Consequently, it is expensive to perform free energy calculations using ab initio QM/MM methods. Semiempirical molecular orbital methods are computationally more efficient and they offer the opportunity to develop specific reaction parameters (SRPs) to improve the accuracy for specific systems (58, 114–116). Because the shape of the PES is usually well represented, an even simpler approach is to add a semiempirical valence bond term such as the London-Eyring-Polanyi-Sato function (54, 117) to correct the errors in the predicted free energies of reaction and activation. This approach has been used in the study of hydride transfer reactions in liver alcohol dehydrogenase (48, 54).

Semiempirical QM/MM methods can be used in what are called dual-level simulations (118–122). In this approach QM/MM energies are separated into a solvent-independent (gas phase) term and a solute-solvent interaction component such that a high-level (HL) method, typically MP2 or DFT, can be used to determine the intrinsic energy of the reactants in the gas phase while the time-consuming free energy calculations are carried out with a lower-level (LL) model. A similar approach is the integrated molecular orbital molecular mechanics (IMOMM) method (123), in which the lower-level calculation is performed by a pure molecular mechanical method rather than by using a combined QM/MM potential. In dual-level calculations, the total potential energy (and free energy) of the system can be separated as follows (118, 122):

$$E_{\text{tot}} = E_{\text{qm}}^{\text{HL}}(\text{gas}) + \Delta E_{\text{qm/mm}}^{\text{LL}} + E_{\text{mm}}, \qquad 4.$$

where $E_{\text{qm}}^{\text{HL}}(\text{gas})$ is the energy of reactants computed at a high level of theory in the gas phase, typically ab initio calculations that include electron correlations, E_{mm} is the molecular mechanical energy of the protein, and $\Delta E_{\text{qm/mm}}^{\text{LL}}$ is the QM/MM interaction energy modeled with a lower-level quantum mechanical method, e.g., the AM1 model (88) combined with the CHARMM force field (38). In this approach, the free energy calculation is carried out using a lower-level QM/MM potential, whereas the high-level quantum mechanical result is made as a posterior correction to the intrinsic (i.e., gas-phase) energy of the quantum mechanical part from the lower-level calculation (118, 122). This energy separation is made possible by using the QM/MM energy decomposition scheme developed previously (76), and the method has been applied to the solvation of organic molecules (118, 119, 122, 124).

Warshel and others have used a valence bond formalism to approximate the electronic structure of the reactants in the enzyme active site (125). In the most

widely used valence bond approach (20, 49, 97, 125–135), computational efficiency is obtained by treating the energies of valence bond configurations with molecular mechanical force fields and using a constant or one-variable exponential function for the resonance integrals (H_{12}); such calculations are denoted as empirical valence bond (EVB) (127, 128). Unlike combined QM/MM methods, the electronic wave function is implicit in the EVB model, and thus the overlap integrals between valence bond states are approximated as zero; the effect of neglecting overlap integrals on the ground-state potential energy surface (PES) is assumed to be absorbed in the parameter-fitting step. The inclusion of a solvation energy term in the diagonal EVB matrix elements provides a way to model reactions in solution and in enzymes (127). The off-diagonal matrix element, H_{12}, is assumed to be environment independent. The EVB method provides a fast analytical procedure for obtaining approximate reactive PESs and has been used extensively (97).

Effective diabatic states such as those used in EVB-type models are not pure valence bond states and they are mixtures of valence bond configurations, which include both covalent and ionic contributions. Although the charge distribution of pure valence bond configurations in ab initio valence bond theory can be described by Lewis resonance structures with charges localized in specific valence bond orbitals, the charge distribution of mixed or partially mixed valence bond states (or effective diabatic states) depends on molecular geometry and environment (28, 136). Although a fixed-charge diabatic valence bond state can be parameterized to model reactions, it is dangerous to infer energetic insights using such diabatic states. It would be possible to develop a semiempirical valence bond model in which empirical charges for individual effective valence bond states vary as a function of reactant geometry, but the functional form and calibration procedure would be complicated.

The EVB method when used as described above is on the border between a classical and a quantum mechanical electronic structure method, but it is considered as a classical method (like molecular mechanics) in this review. It is, however, possible to use valence bonds as a quantum mechanical method, as discussed next.

A mixed molecular orbital and valence bond (MOVB) method was recently introduced (28, 136); it combines and extends many features of combined QM/MM techniques as well as ab initio valence bond theory. In the MOVB method, the effective diabatic state is treated by a block-localized wave function theory (137, 138), corresponding to the traditional Lewis resonance structures. Because the block-localized wave function approach is based on an ab initio molecular orbital wave function that corresponds to a mixed valence bond state, the geometrical dependence of gas-phase charge distribution and solute-solvent electronic polarization are naturally included in the MOVB method's Hamiltonian matrix (28, 136). Thus, the significance of omitting all or some of these factors can be systematically investigated without the need to empirically adjust parameters (28, 136).

Schmitt & Voth described a multistate empirical valence bond model for proton transport in water (139, 140). The approach extends the two-state EVB method by introducing an exchange charge distribution in the off-diagonal terms to mimic

transition dipole moments. Inclusion of these exchange (or transition) charges, which is also present in MOVB (28), led to qualitatively different results in modeling proton transport in water in comparison with a similar approach that excluded such explicit off-diagonal solute-solvent interactions (139, 140).

In another valence bond approach a multiconfiguration molecular mechanics method was proposed with a systematic parameterization scheme for the off-diagonal element (141, 142). This method can accurately reproduce ab initio energies and gradients and does not suffer from the limitation of the formalism to matrices of order 2 in that it can be systematically converged to reproduce high-level calculations. In this respect, it is a systematic fitting tool based on the valence bond formalism rather than an approximate valence bond calculation per se.

Potential of Mean Force

Next we turn our attention from the electronic structure considerations that yield the PES to the nuclear dynamics. The first challenging goal is to obtain an accurate estimate of $\Delta G^{\neq}(T)$ by computing the potential of mean force (PMF) along the reaction coordinate. Two methods are generally used in the calculation of PMFs for reactions in solution and in enzymes, the umbrella sampling (35) technique and the free energy perturbation theory (36); these are reviewed elsewhere (143). Because these calculations are often carried out using purely classical mechanics, zero-point energy and effects of the quantization of vibrational motion are neglected. It has been shown in several studies (48, 49, 52, 54, 58, 144, 145) that omission of these quantum effects can lead to significant errors in computed free energies of activation, particularly in systems involving hydrogen transfer. Thus, it is desirable to make quantal corrections to the classical mechanical-PMF or to perform simulations that directly include nuclear quantum mechanical effects.

To this end, our groups (48, 145) have developed a convenient procedure to include the effect of quantization of molecular vibrations in free energy calculations. In this method, the quantal PMF is related to the classical PMF of Equation 3 by

$$W_{QC}(T, z) = W_{CM}(T, z) + \Delta W_{vib}(T, z), \qquad 5.$$

where $\Delta W_{vib}(T, z)$ is an ensemble average of the instantaneous harmonic approximation to the quantal correction to the classical vibrational free energy for vibrational modes orthogonal to the reaction coordinate, and the subscript QC denotes "quasiclassical" and specifies the fact that tunneling and other quantum effects on the reaction coordinate, z, are excluded. The procedure involves instantaneous normal mode analysis based on local harmonic approximations, and this should be more accurate than using true normal mode analysis at a single local minimum. In applying Equation 5, the lowest vibrational modes corresponding to low-frequency vibrational motion, for which the classical approximation should be adequate, are omitted in the calculation of $\Delta W_{vib}(T, z)$. The constraint that the modes included are orthogonal to z can be achieved by a projection operator (48, 145). To evaluate the QC free energy of activation, quantum corrections must also be made to the

$G_{CM}^R(z)$ term in Equation 2. A procedure for estimating the required frequency ω_R of the reaction-coordinate mode of the reactant has been presented (48).

Free energy simulations of model proton shifts in water as well as enzymatic hydrogen transfer reactions in a number of enzymes indicate that inclusion of quantum vibrational free energy contributions reduces the classical barrier height by 2–4 kcal/mol and that more degrees of freedom than those associated with the migrating atoms are needed in these calculations (49, 52, 54, 145, 146).

Another method for including quantum effects on vibrations is the path integral technique (147). In this approach the ensemble averages for the quantum system can be obtained by carrying out a classical simulation in which the quantized particles are represented by ring polymers of classical particles. To determine the PMF, it has been proposed to define the positions of the quantized particles and hence the value of the reaction coordinate using the average positions (148–154), or centroids, of the ring polymers, leading to a method called path integral quantum transition state theory (TST). Although this approach has been successful for some problems and was applied to an enzyme reaction (53), it has been noted that difficulty exists for asymmetric reactions at low temperature (154–158). An algorithm has been proposed in which classical free energy calculations are performed first, and then quantum corrections are added by a path integral calculation with the centroids constrained at the classical atom positions (146, 153). This approach has been called the quantum-classical path (QCP) method and has also been applied to enzymes (133, 135, 146, 153). A path integral approach that does not use the centroid concept has been shown to overcome the deficiencies of the centroid-based approach but has not so far been applied to enzymes (157). A path integral method designed to reduce the variance in sampling has also been proposed (158a). It is interesting to note that Tuckerman & Marx (159), who employed a centroid path integral method in the study of the proton transfer reaction of malonic acid, found that the reaction rate is underestimated by a factor of two if only the transfer proton is treated quantum mechanically in the framework of classical heavy atoms, compared with a full path integral quantum mechanics treatment.

Recently, Billeter et al. (49) used a hybrid approach to study enzymatic hydrogen transfer reactions. In this approach the free energy of activation is first calculated by a mixed quantum/classical molecular dynamics (MQCMD) method, and then a transmission coefficient is added by molecular dynamics with quantum transitions (MDQT). We discuss the MQCMD step here and the MDQT step in the next section. In the MQCMD step the nuclear degrees of freedom are divided into a quantal subset and a classical subset; the quantal subset is treated by using the Fourier grid Hamiltonian multiconfigurational self-consistent field method (160, 161) to calculate a three-dimensional hydrogen vibrational wave function, which is expressed as a linear combination of products of one-dimensional wave functions. Since the one-dimensional basis functions are directly represented on a cubic grid, the numerical calculation of the vibrational wave function requires knowledge of the potential energy and forces at each grid point for each dynamics integration step. The latter calculations are the computational bottleneck in

the Fourier grid Hamiltonian multiconfigurational self-consistent field approach because a large number of grid points and memory space are needed (49). To generate the quantum PMF from classical simulations, a free energy perturbation approach analogous to the QCP algorithm (153) is used to yield the free energy difference between the quantum (Fourier grid Hamiltonian multiconfigurational self-consistent field) and classical EVB-mapping potential along the reaction coordinate.

In an approach called the quantum mechanical–free energy method (162–167) or the "solvated gas-phase" approach (135), free energy perturbation theory is used to add environmental free energies (i.e., bath free energies) along gas-phase reaction paths (162–168). This involves free energy perturbation on the molecular mechanics subsystem for a fixed quantum mechanical subsystem. An advantage of this method is that it allows high-level quantum mechanical calculations for the gas phase portion of the problem, but a serious disadvantage is that it does not treat the effect of the bath on the primary subsystem self-consistently. This effect is included to some extent by fixing certain anchor atoms of the quantum mechanical model to the protein coordinate frame (162, 169). However, we do not consider this method further because it does not introduce quantum mechanics into a full enzymic simulation.

Dynamics and Tunneling

Whereas the previous section was concerned with quantum effects within the transition state hypersurface, in which the reaction coordinate is missing, this section focuses on the reaction coordinate. However, we note that the calculation of free energy of activation and dynamical effects are not independent of each other. There are two major factors contributing to the transmission coefficient, $\gamma(T)$: (*a*) dynamical recrossing, which can be estimated classically and is discussed above, and (*b*) nuclear tunneling and other quantum effects on the reaction coordinate that are missing in the calculation of the PMF. It can be difficult, however, to separate quantum effects on the reaction coordinate from those on other degrees of freedom if path integral or quantum-classical molecular dynamics calculations are carried out. To a certain degree, the effect of the nuclear tunneling contributions is absorbed into the computed PMF in these methods. Thus, methods discussed in the previous section are often related to techniques reviewed below. From a more general perspective, we note that any reliable approach to calculating tunneling effects must be multidimensional to take account of the nonseparability of the reaction coordinate.

We can distinguish three ways to include quantum mechanical effects on reaction-coordinate motion. The first category involves dynamical calculations that do not involve transition state theory; an example of such an approach that has been applied to enzyme dynamics is the quantum-classical molecular dynamics method reviewed below. The second category includes quantal TST methods that recognize the finite spatial extension of a quantum mechanical transition state

along the reaction coordinate (the infinitesimal thickness of a classical transition state hypersurface violates the Heisenberg uncertainty principle). In such methods, tunneling contributes to the free energy of activation. An example of this approach is path-integral–quantum TST, including the QCP algorithm, discussed in the previous section. The third way to include quantum effects involves first calculating a free energy of activation in which reaction coordinate motion is separated from all other degrees of freedom normal to it. In this technique, introduced above, the free energy of activation is quasiclassical because the progression coordinate is classical and the other degrees of freedom are quantal. The dynamical recrossing and quantum effects on the reaction coordinate, including the effects of nonseparability, are treated by means of a transmission coefficient. An example of this approach is ensemble-averaged variational transition state theory with multidimensional tunneling (EA-VTST/MT) (48, 59) for estimating transmission coefficients of enzymatic reactions. The MQCMD/MDQT method (49) lies between categories 2 and 3.

Bala et al. (55, 170) described a mean-field quantum-classical molecular dynamics model in which the dynamics of the quantum subsystem is described by the time-dependent Schrodinger equation, whereas the rest of the system is treated by Newtonian dynamics. The coupling between the quantum subsystem and the classical atoms is modeled by a mean-field method through extended Hellman-Feynman forces. The method has been used to study a proton tunneling process in the active site of phospholipase A_2 (55). Other mean-field approaches include the time-dependent self-consistent field method (171, 172) and the density matrix evolution technique (173, 174).

The MQCMD/MDQT technique of Billeter et al. (49, 175) uses reactive flux for computing the transmission coefficient for enzyme reactions. The MQCMD step is discussed in the previous section. In the second step the MDQT surface hopping method (160, 175–178) is used to calculate a transmission coefficient. Although MDQT was originally developed for treating electronically nonadiabatic transitions, it is the nuclear motion of hydrogen that is treated quantum mechanically in applications to enzymes. The method includes both vibrationally adiabatic and vibrationally nonadiabatic motions of the hydrogen, as does the EA-VTST/MT method described below. For calculating rate constants, the MDQT method uses a fictitious surface hopping algorithm that does not depend on the quantum amplitude for backward trajectories. Then, forward trajectories are propagated with the true surface hopping method by integrating the quantum amplitude of the same trajectories. This approach assumes a Boltzmann distribution of vibrationally adiabatic states at the transition state dividing surface for both the fictitious and true surface hopping algorithms (175).

In our own approach, which is EA-VTST/MT, the net transmission coefficient is approximated as (48, 58)

$$\gamma(T) = \langle \kappa(T)\Gamma(T) \rangle_{\neq} \cong \frac{1}{M} \sum_{i=1}^{M} \kappa_i(T)\Gamma_i(T), \qquad 6.$$

where the brackets $\langle \cdots \rangle_{\neq}$ represent an ensemble average over transition state configurations at temperature T, $\Gamma(T)$ accounts for dynamical recrossing, $\kappa(T)$ accounts for tunneling through the effective barrier and nonclassical diffractive reflection from the barrier top, i denotes a particular member of the quasiclassical transition state ensemble, and M is the total number of configurations that have been sampled in the calculation. The ensemble of transition state configurations can be generated during the PMF calculation using umbrella sampling (58; M. Garcia-Viloca, C. Alhambra, D.G. Truhlar, J. Gao, unpublished manuscript) or in a separate molecular dynamics simulation with the constraint that the reaction coordinate corresponds to the transition state value (52, 54). The progress coordinate z that defines this ensemble can be either a combination of internal coordinates or a diabatic energy-gap coordinate representing collective solvent motions. In our work so far, we have used the difference of the breaking and making bond distances. For each configuration i in the transition state ensemble, the recrossing factor $\Gamma_i(T)$ is evaluated by an embedded cluster (19, 21, 48, 179) formalism in which an improved choice of the transition state hypersurface is determined using quantized variational TST (VTST) for that individual configuration, and the "tunneling factor" $\kappa_i(T)$ is also computed in the same calculation by a semiclassical multidimensional tunneling (MT) approximation, either the small-curvature tunneling approximation (180) or the microcanonically optimized MT approximation (181). The latter involves choosing at each tunneling energy the better of the small-curvature (180) and large-curvature (182, 183) tunneling approximations.

For each configuration i in the transition state ensemble, the system is partitioned into a primary zone and a secondary zone. The primary zone consists of N_1 atoms, which can be the same quantum mechanical fragment as that used in the combined QM/MM potential or a different set of atoms, and they have kinetic energy. The secondary zone represents the rest of the system, which is kept frozen in the calculation of an isoinertial minimum energy path (MEP) for the embedded primary zone (48). The progress variable along the MEP becomes the reaction coordinate, denoted as s to be distinguished from z used in the PMF calculation. The calculation yields a generalized transition-state free energy of activation $\Delta G^{GT}(T, s_i)$ and a semiclassical transmission coefficient $\kappa(T)$ by methods fully described in previous work (5, 180–190). In a canonical ensemble of primary systems interacting with its frozen environment the minimum-flux dividing hypersurface is the one with maximum $\Delta G^{GT}(T, s_i)$, which is located at $s_i = s_i^{\neq}$ (this defines $s_i^{\neq}$). The equilibrium classical flux is reduced relative to the dividing hypersurface that corresponds to $\Delta G_{QC}^{\neq}(T)$, which is the quasiclassical free energy of activation described in the previous section, by a factor of (19, 21, 48)

$$\Gamma_i(T, z) = \exp\{-\beta[\Delta G^{GT}(T, s^{\neq}) - \Delta G_{QC}^{\neq}(T)]\}. \qquad 7.$$

Note that $\Delta G^{GT}(T, s_i)$ is normalized so that it equals $\Delta G_{QC}^{\neq}(T)$ when $z(s_i) = z_i^{\neq}$. Equation 7 is called the quasiclassical transmission factor (48).

The net effect of quantum contributions on the reaction coordinate motion, relative to value reduced by Equation 7, is given by the semiclassical transmission

coefficient $\kappa_i(T)$. The methods used for tunneling approximate the quantum mechanical transmission probabilities by the Wentzel-Kramers-Brillouin approximation (191) in terms of imaginary action integrals; such a treatment is called semiclassical because it uses classical variables (or their analytic continuation to complex momenta) to approximate quantum mechanical dynamics (192). The net effect of $\kappa_i(T)$ is usually to increase the reactive flux because the tunneling has a larger Boltzmann weight than does the nonclassical reflection. Note that $\kappa_i(T)$ is an implicit function of $z^{\neq}$, the location of the maximum PMF along the reaction coordinate z, because it is computed in the framework of the transition state configurations chosen at $z^{\neq}$, and it is an implicit function of $s_i^{\neq}$ because it gives a net factor relative to the rate constant reduced by Equation 7.

Calculations employing Equation 6 may be carried out using either the static-secondary-zone (SSZ) approximation or the equilibrium-secondary-zone (ESZ) approximation. In the SSZ approximation the effective free energy profile for the calculation of $\Gamma(T)$ and the effective tunneling potential for the calculation of $\kappa(T)$ are evaluated with a frozen secondary zone. Although the frozen bath approximation is reasonable for the short timescale of barrier crossing for enzymatic reactions, especially for hydrogen transfer reactions, the SSZ approximation does not include dynamical and entropic contributions from the surrounding protein in the transmission coefficient. This is corrected in an ESZ approach (48), in which these effective quantities also include thermal energetic and entropic contributions from the secondary zone; the latter are obtained by additional secondary-zone free energy calculations along the MEP for each configuration in the transition state ensemble (48).

The SSZ and ESZ versions of the EA-VTST/MT method were first presented in a paper on the study of liver alcohol dehydrogense (LADH) (48). The SSZ model was subsequently applied to methyl amine dehydrogenase (58) and xylose isomerase (M. Garcia-Viloca, C. Alhambra, D.G. Truhlar, J. Gao, unpublished manuscript). We also employed a preliminary version of this approach in our earlier papers on enolase (52) and LADH (54), but this review covers details only for the latter more satisfactory EA-VTST/MT method.

It is useful to compare the MQCMD/MDQT (49) and EA-VTST/MT (48) approaches to estimating the free energy of activation and transmission coefficient because both appear to be very promising. Both methods are based on Equation 1 and incorporate the desirable feature that the free energy difference between the transition state and reactant is evaluated by computing the potential of mean force along a progress variable z. Both methods include recrossing and quantum effects in the transmission coefficient; this is very efficient because such effects are more localized in time and space than the semiglobal dynamics that determine $\Delta G^{\neq}(T)$. Because the inclusion of a recrossing correction can make up for a nonoptimal choice of a transition state hypersurface, such methods can in principle be very accurate. The accuracy ultimately depends on the quality of the transmission coefficient and the accuracy of the PES. The recrossing estimated using the MDQT method has the advantage of involving full dynamics but the disadvantage of not quantizing all particles owing to computational cost (so far only one particle

has been quantized). Furthermore, in weakly coupled cases the MDQT algorithm does not treat the quantized and classical particles fully self-consistently owing to frustrated hops (178, 193). The dynamical recrossing correction estimated by using EA-VTST/MT in the embedded cluster approximation quantizes all but one degree of freedom in the primary zone (which may therefore involve ∼100 or more quantized degrees of freedom) but involves extra approximations for the secondary zone. Both approaches include tunneling, although the MDQT technique includes tunneling effects in the calculation of the PMF. The EA-VTST/MT method incorporates tunneling contributions in the transmission coefficient. The VTST/MT method has been very extensively validated against accurate quantum dynamics for smaller systems (5, 9, 10, 187, 194, 195).

In practice, the MQCMD/MDQT approach has been applied with a discrete energy gap coordinate for z, whereas EA-VTST/MT has used internal coordinates. However, these choices are not intrinsic restrictions to the methods; these two choices for the reaction coordinate have recently been compared for nonenzymatic reactions in polar media (28, 136, 196). In another study MDQT and VTST/MT were compared for a proton transfer in a polar medium (196a).

APPLICATIONS

We divide the discussion of applications into two sections: those that have quantum effects in the nuclear dynamics and those that do not. In the latter we include only studies involving a quantum mechanical treatment of electronic structure, and we further divide these studies into those that use statistical mechanics to compute free energies and those that do not. The latter deal only with potential energies. Simulations involving only classical mechanical dynamics with molecular mechanics potential functions are not included in this review, even though—taking a broader view—most molecular mechanics potentials used for biochemical simulations are originally fit using at least some input from quantum mechanical electronic structure calculations. Furthermore, although much can be learned from analytic few-dimensional models and general discussions or calculations on model systems that do not explicitly include the specific enzyme (or most of it), such models are not reviewed here. One problem with such models is that they often make unrealistic assumptions motivated by the goal of simplifying the problem. Our subject here is the emerging field of quantum mechanical methods for modeling detailed interactions and the resulting dynamics in specific enzymes with the atoms of the enzyme explicit. For lack of space, we omit discussion of electron transfer reactions.

Quantum Treatments of Nuclear Dynamics

Systems are discussed in this subsection in roughly chronological order.

LACTATE DEHYDROGENASE Hwang et al. (197) used the quantum-classical path (QCP) method to calculate the free energy of activation profile as a function of an energy-gap reaction coordinate (125) for the hydride transfer from nicotinamide

adenine dinucleotide hydride (NADH) to pyruvate catalyzed by lactate dehydro-genase. The potential energy function was modeled by empirical valence bond (EVB) with an empirical exponential function coupling the valence bond states. Quantum effects on nuclear motion lowered the free energy of activation from 12 to 9 kcal/mol.

CARBONIC ANHYDRASE   Hwang & Warshel (146) used the QCP method to calcu-late the free energy of activation profile for proton transfer between water molecules catalyzed by the zinc metalloenzyme carbonic anhydrase. The potential was mod-eled by EVB. They treated six atoms as quantal and found that quantum nuclear motion effects lower the free energy of activation from 12 to 10.5 kcal/mol (146). They calculated a kinetic isotope effect (KIE) of 3.9 (146, 198).

PHOSPHOLIPASE A$_2$ (PLA$_2$)   Bala et al. (55) applied the quantum-classical molec-ular dynamics method to study proton transfer from water to histidine with nearly simultaneous nucleophilic attack of the resulting OH$^-$ on the carbonyl carbon atom of a phospholipid substrate, as catalyzed by PLA$_2$. The PES was modeled by an approximate valence bond method that is similar to EVB but uses density functional theory (DFT) calculations instead of empirical data to parameterize the valence bond coupling. Quantum nuclear motion effects lowered the average barrier from 2.5 kcal/mol to 0.5.

ASPARTIC TRANSCARBAMOYLASE   Pawlak et al. (199) studied the reaction between carbonyl phosphate and aspartate catalyzed by aspartic transcarbamoylase. The re-actants were treated by the PM3 model in the rigid field of an optimized structure of the active site residues, whose interaction with the quantum mechanical subsystem was modeled by atomic potential charges determined in a supermolecular calcula-tion involving 490 atoms. Proton transfer was found to be slightly more advanced in the flexible model of the active site. Kinetic isotope effects were calculated by conventional TST with quantized harmonic vibrations and unit transmission coeffi-cient using the rigid active site. Both wild-type enzyme and a mutant were studied.

GLUTATHIONE REDUCTASE   Transition states were optimized for hydride transfer from nicotinamide adenine dinucleotide phosphate hydride (NADPH) to a flavin cofactor as catalyzed by glutathione reductase (51). The quantum mechanical system was treated by AM1, and the molecular mechanical part of the calculation employed CHARMM and TIP3P; the subsystems were joined by link atoms. KIEs were calculated by conventional TST with quantized harmonic vibrations and a Wigner transmission coefficient. The latter is as large as 4.2, and the authors noted that Wigner approximation is not reliable for such a large transmission coefficient (51).

ENOLASE   Alhambra et al. (52) studied the proton transfer from 2-phospho-D-glycerate to the ε-nitrogen of Lys345 in the active site of the homodimeric enzyme

enolase. The mechanism of the enolase reaction is particularly interesting because the rate-limiting step involves the abstraction of a proton from a weak carbon acid through electrostatic stabilization of the carbanion intermediate by two magnesium ions in the active site. The PES was modeled with 25 AM1 atoms connected to an 8863-atom CHARMM22/TIP3P environment through generalized hybrid orbital (GHO) boundary atoms (99). Umbrella sampling simulations were carried out using molecular dynamics to determine the potential of mean force (PMF) along a reaction coordinate defined as the difference between the making and breaking bond distances of the transferring proton. Then, a molecular mechanical simulation with strong harmonic restraints of the reaction coordinate at the transition state value was performed to generate a representative enzyme structure for dynamics calculations. Subsequently, the system was partitioned into a primary zone and secondary zone to yield an isoinertial minimum energy path (MEP) for 25 quantum mechanical atoms in a bath of 8863 classical atoms. The reactant, transition state, and product were optimized, and the MEP of the proton transfer reaction was calculated and used as the basis for VTST/MT calculations of the rate constant and the deuteron KIE. Quantum effects on nuclear motion decreased the free energy of activation from 16.8 kcal/mol to 14.4 and increased the rate constant by a factor of 56 (a factor of 34 owing to quantizing vibrational motion orthogonal to the MEP and an additional factor of 1.7 from adding quantum effects—primarily tunneling—to the reaction coordinate) (52). Good agreement with the experimental KIE was achieved only by including the isotope dependence of the dynamical bottleneck location.

DIHYDROFOLATE REDUCTASE   Castillo et al. (200) studied hydride transfer from NADPH to 7,8-dihydrofolate catalyzed by dihydrofolate reductase. The PES was modeled by QM/MM with link atoms between a 53-atom AM1 region and a CHARMM24 region. A saddle point was optimized, and KIEs were calculated by conventional TST with harmonic quantized vibrations and no tunneling. The hydrogen/deuterium (H/D) KIE was calculated to be 3.7–3.9, compared with an experimental value of 3.0.

GLYOXALASE I   Feierberg et al. (133) studied the proton abstraction of a hemithioacetal by Glu172 of the zinc metalloenzyme glyoxalase I. The hemiacetal results from binding of methylglyoxal substrate to a glutathione cofactor. The PES was modeled by the EVB method. The free energy of activation as a function of an energy-gap reaction coordinate was calculated by the QCP method, and quantum effects on nuclear motion were found to lower the free energy of activation from $\sim$14.8 to $\sim$12.3 kcal/mol. H/D and hydrogen/tritium (H/T) KIEs of 5 $\pm$ 1 and 8 $\pm$ 3 were calculated, compared with gas-phase values of 5–6 and 9–12, respectively.

LIVER ALCOHOL DEHYDROGENASE (LADH)   One of the most extensively studied enzymes is LADH (48, 49, 54, 135, 201), which catalyzes the reversible conversion of an alcohol to an aldehyde in the active site of a ternary complex that requires a nicotinamide adenine dinucleotide (NAD^+) coenzyme. The chemical

step is hydride transfer from the alcoholate anion to NAD^+. A catalytic Zn ion is present in the active site, which is coordinated to the alcoholate form of the substrate and one His and two Cys residues. The work of Klinman and coworkers provides strong experimental evidence for hydrogen tunneling in the chemical step in alcohol dehydrogenation by wild-type LADH, mutant LADH, and yeast alcohol dehydrogenase (202, 203). Two important questions to be addressed are (*a*) Can kinetic isotope effects be accurately predicted for such enzymatic reactions? and (*b*) To what extent does quantum mechanical tunneling contribute to the rate enhancement in LADH? LADH catalysis has now been studied with explicit enzyme and nuclear-motion quantum effects by three groups (48, 49, 54, 135).

In our first study of LADH (54) the hydride transfer reaction was successfully studied with a multidimensional semiclassical treatment of the KIEs using the same theory that was applied to the enolase reaction described above (52), but for LADH we also included statistical averaging over several secondary-zone configurations. Subsequently, we developed the more complete method outlined above and in an account article (59) and described in detail elsewhere (48), and we applied the new theory to the LADH reaction. We summarize the latter simulation (48) here. [We note that the inclusion of protein motion effects on the transmission coefficient in the new calculation (48) makes a quantitative but not a qualitative change as compared with the results of the earlier (54) calculation.]

Unlike the enolase case, in which the semiempirical AM1 model was adequate, the hydride transfer in LADH directly involves a Zn ion. As a result, energetic quantities obtained from semiempirical (AM1 or PM3) calculations are not in good accord with available experimental data and high-level ab initio results for model reactions. To correct this, we added a semiempirical valence bond term to a QM/MM calculation based on 21 AM1 atoms joined to 5506 CHARMM22/TIP3P atoms by GHO boundary atoms (48). The semiempirical valence bond parameters were adjusted so that the combined potential reproduces the MP2/6-31 + G^* potential energy surface for the model reaction between Zn-complexed benzyl alcoholate and NAD^+ in the gas phase. The resulting PES shows that the active site of LADH is characterized by a delicate hydrogen-bonding network as well as hydrophobic interactions, which all make important contributions to the dynamics of the hydride transfer process. We obtained a quasiclassical free energy of activation of 14.7 kcal/mol for oxidation of benzyl alcoholate, whereas the calculated maximum of the classical mechanical free energy of activation curve as a function of the difference between the making and breaking hydride bond distances is 16.5 kcal/mol; the difference shows the importance of quantum mechanical vibrational free energies. The experimental phenomenological free energy of activation is 15.6 kcal/mol.

The transmission coefficient γ was averaged using the EA-VTST/MT method in two ways over 18 equilibrium configurations in the transition state, for each of which we determined isoinertial MEPs with various isotopic substitutions at the primary and secondary positions of the hydride transfer reaction in LADH (48). In the SSZ approximation the dynamic contributions of the surrounding

protein-solvent bath are excluded. These effects on the shape of the potential surface and the position of the transition state are incorporated in our ESZ algorithm by computing the free energy change of the secondary zone system along the reaction paths determined in the SSZ stage. Average values of $\gamma^{(SSZ)} = 2.5$ and 2.4 were obtained for the hydride transfer from the microcanonically optimized multidimensional-tunneling and small Λ-curvature-tunneling approximations in the SSZ approach; the average transmission coefficient was increased to $\gamma^{(ESZ)} = 4.1$ by including the protein dynamics contributions. These results indicate a modest increase in the rate constant owing to quantum mechanical tunneling.

It is essential to include quantum mechanical tunneling effects to obtain accurate KIEs. The result is particularly striking for the secondary H/T KIE, which is much larger than the value one would expect from the H/D secondary KIE on the basis of vibrational partition functions. The calculated H/T secondary KIE is 1.36, in good agreement with the experimental value of 1.33.

What is the origin of the exaltation of the secondary H/T KIE in the LADH reaction? It results from tunneling effects that increase the H/T secondary KIE by 17% in stage 2 calculations. (Incorporating the dynamic contributions of the surrounding protein-solvent bath in the ESZ calculation did not have a large effect.) Analysis (54) of the vibrationally adiabatic ground-state potential barrier for one of the SSZ configurations shows that it is not well approximated by a parabola and that tunneling along the MEP would give rise to an 8% effect in the ratio of the computed transmission coefficients; another 8% comes from reaction-path curvature, which is larger for hydrogen than for tritium in the region of the dominant tunneling paths. Inclusion of nuclear motion tunneling effects for the perprotio case lowers the free energy of activation from 14.7 kcal/mol to 13.9.

For LADH we compared small-curvature and large-curvature tunneling algorithms. Although the large-curvature algorithm (and hence microcanonically optimized MT) is often required for accurate results in gas-phase bimolecular reactions involving the transfer of a light particle between two heavy moieties (9, 142, 186, 194, 204), we have previously pointed out (205) that the curvature for heavy-light-heavy unimolecular reactions (such as the reactions of enzyme-substrate complexes) need not be large. Thus, it is not known how important large-curvature tunneling will turn out to be for enzymatic reactions. We found that large-curvature tunneling is not important for the LADH reaction in this study.

Hammes-Schiffer and coworkers (49, 134, 206) studied the reaction of benzyl alcoholate anion using the MDQT approach with one nucleus-treated quantum mechanical. The PES was an EVB potential based on a modified GROMOS united-atom force field with four explicit hydrogen atoms and with a constant value for the coupling matrix element H_{12}. The transition state ensemble was identified by classical mechanical and MDQT calculations of the free energy profile as a function of an energy gap. Quantum mechanical nuclear-motion effects lower the free energy of activation from 17.2 kcal/mol to 15.4. Two sample MDQT trajectories were presented to illustrate how one could include recrossing effects as a transmission coefficient (49).

Villà & Warshel applied the QCP method to these problems (135), assuming that the classical and quantum mechanical transmission coefficients are identical. They presented a preliminary calculation of the free energy of activation profile along an energy-gap coordinate. Quantum effects on nuclear motion lowered the free energy of activation from 14.5 to 12 kcal/mol.

TRIOSE PHOSPHATE ISOMERASE   Karplus and coworkers studied the conversion of dihydroxyacetone phosphate to D-glyceraldehyde-3-phosphate by triose phosphate isomerase. QM/MM was used to calculate free energy barriers by adding quantized vibrational free energies to B3LYP single-point potential energies at structures optimized with a smaller quantum mechanical region (207).

METHYL AMINE DEHYDROGENASE   Methyl amine dehydrogenase oxidizes primary amines to an aldehyde and ammonia by using the tryptophan tryptophylquinone prosthetic group as a cofactor. The rate-limiting step for the half reaction in which tryptophan tryptophylquinone is reduced corresponds to the breakdown of an iminoquinone intermediate by proton transfer from the carbon atom of a methylimino moiety on the prosthetic group to an Asp residue of the enzyme. Experimental studies (208, 209) have found large primary KIEs in comparison of CH_3NH_2 to CD_3NH_2.

Faulder et al. (57) studied this reaction with a QM/MM PES in which a 31-atom region described by PM3 is joined by link atoms to an environment described by AMBER. The reactant structure was optimized to a local minimum; then the molecular mechanical region was frozen and a transition state was optimized in the reactant environment. This was used as a starting point for calculating a 31-atom MEP in the frozen environment. This was used in a canonical variational theory/small-curvature tunneling calculation that yielded a KIE of 11.1 at room temperature, compared with a conventional TST value (without tunneling) of 6 and an experimental value of 18. The overbarrier mechanism was predicted to contribute about 4% of the observed rate, with 96% owing to tunneling.

Our own study included a subset of 48 atoms in the quantum mechanical region that is treated by the semiempirical PM3 model with specific reaction parameters (SRPs) determined for the proton transfer reaction in methyl amine dehydrogenase (58). The SRPs were only used for the methyl carbon of the substrate, methyliminoquinone, and their values were adjusted to yield good agreement with ab initio MP2/6-31G* and B3LYP/6-31G* results for two model reactions. An additional 10,977 atoms, of which 7248 were protein atoms and 3729 were from 1243 solvent water molecules, were included in the molecular mechanical part of the system, which was joined to the quantum mechanical part by GHO boundary atoms (99). Atoms within 24 Å of the reaction center were included in the dynamics calculations, and the transmission coefficients were determined by using the static-secondary zone (SSZ) approximation.

From the classical mechanical PMF, the estimated free energy of activation is 20.3 kcal/mol for the proton transfer reaction from methyliminoquinone to Asp-76.

Inclusion of quantum mechanical vibrational free energies averaged over 400 instantaneous configurations corresponding to the reactant and transition region and the effect of the average Γ (the dynamic recrossing transmission coefficient) reduces the effective barrier height to a value of 17.1 kcal/mol (58). The latter result, which does not include quantum mechanical tunneling contributions, is the quasiclassical free energy of activation. The net effect of including tunneling and recrossing is to further lower the energy of activation by 2.5 kcal/mol to 14.6. Thus, the overall lowering of the free energy of activation by including quantum effects in the nuclear motion is 5.7 kcal/mol.

Our calculations indicate that overbarrier processes contribute only about 1% to the rate, with tunneling accounting for the rest. We calculated a KIE of 17 in excellent agreement with the experimental value of 18 (208, 209). Conventional TST without tunneling yielded a KIE of only 6.

XYLOSE ISOMERASE   Xylose isomerase converts the aldose D-xylose to the ketose D-xylulose and, as summarized by Hu et al. (210), it is believed to operate by catalyzing a 1,2-hydride shift in the ring-opened aldose. Two Mg^{2+} cofactors play a role (211, 212). One of the two magnesium ions (Mg-1) in the active site is tightly held by the protein, whereas the second magnesium ion (Mg-2) is mobile; Mg-2 occupies two possible positions that are 5.4 and 3.8 Å from Mg-1, respectively, in the active site of xylose isomerase complexed with D-glucose (213). It is the latter configuration (shorter Mg-Mg separation) that corresponds to the active form of the enzyme for the hydride transfer step in xylose isomerase. We (M. Garcia-Viloca, C. Alhambra, D.G. Truhlar, J. Gao, unpublished manuscript) found by molecular dynamics simulations that the two magnesium ions move apart again as the hydride transfer reaction takes place. Thus, there is a breathing motion of Mg^{2+} ions that mediates the proton and hydride transfer reactions in xylose isomerase. This reaction is a prototypical example for understanding the role of metal ions in catalysis. Two groups have simulated the reaction including quantum effects on nuclear motion.

Nicoll et al. (56) used a QM/MM PES in which a 42-atom system described by PM3 is joined by link atoms to an environment described by AMBER. Kinetic isotope effects were calculated by the canonical VTST/small-curvature tunneling approximation for a single 42-atom MEP in a fixed environment. The room temperature H/D KIE was found to be 6.3, compared with a nontunneling result of 3. Adding corrections from a transition state optimized with B3LYP/6-31G changed the canonical VTST/small-curvature tunneling KIE to 5.8.

The results from our own preliminary molecular dynamics simulations (59) of the Michaelis complex between xylose isomerase and xylose were consistent with the mechanism proposed by Whitlow et al. (214). In this mechanism the 2-hydroxy proton of the substrate is first transferred to a hydroxide ion that is ligated to Mg-2, which leads to the replacement of one of the bidendate interactions between Mg-2 and Asp254 by an interaction with the 2-alkoxide anion. Concomitantly, Mg-2 migrates about 1 Å toward Mg-1 to resume its second position described

above; this is the active configuration for the hydride transfer step, and the carbonyl group of the substrate becomes a ligand to Mg-2, replacing the neutral Asp256. We proposed that Asp256 is protonated after abstracting a proton from the water molecule, which is the base for abstracting a proton from the 2-hydroxy group of the xylose.

We used a potential that includes a simple valence bond potential adjusted to match the MP2/6-31 $+$ G* results for a model hydride transfer reaction in the gas phase and then further refined on the basis of the experimental overall k_{cat} for the enzymatic reaction. Tests showed that QM/MM calculations with a 19-atom quantum mechanical subsystem agreed well with calculations based on a 79-atom quantum mechanical subsystem that includes the magnesium ions in the quantum mechanical region, so the final calculations were based on the former. The quantum mechanical subsystem was joined to a CHARMM/TIP3P environment (38, 215) by GHO boundary atoms.

Inclusion of quantum effects in the nuclear motion lowered the free energy of activation from 25.0 kcal/mol to 22.6. The calculated KIE is 3.8 at 298 K, in general agreement with experimental values in the range of 2.7–4.0 at 333 K (216–218). Tunneling accounts for about 90% of the rate.

VIRAL NEURAMIDASE   Thomas et al. (53) carried out PMF calculations for the formation of the covalent intermediate catalyzed by viral neuramidase (53). They chose the bond length of one of the two bonds being made as the reaction coordinate. They also used path integral methods to estimate the quantum effects on this step. In the path integral calculations two oxygen atoms and one hydrogen atom were treated as quantum particles; this reduces the free energy of activation from 5.3 kcal/mol to 3.8.

Other Applications with Quantum Electronic Structure and Statistical Mechanics

Much useful information can be obtained from studies that use quantum mechanical electronic structure calculations to calculate PMFs along enzyme reaction paths, transition state theory rate constants, or other dynamical variables based on ensemble averaging, even when quantum effects are not included in the nuclear motion. This section reviews such studies, in alphabetical order of enzyme.

ACETOHYDROXY ACID ISOMEROREDUCTASE   Proust-De Martin et al. (219) used link-atom QM/MM to calculate free energy profiles for the alkyl migration/proton transfer step catalyzed by the Mg-enzyme acetohydroxy acid isomeroreductase. Models with 18–63 quantum mechanical atoms were explored. The quantum mechanical method was AM1. Electrostatic effects were found to be important. The calculated ΔG_{act} is 38 kcal/mol, which is 2–4 times higher than experiment.

CATECHOL O-METHYLTRANSFERASE   Kollman and coworkers (163, 164, 167) applied the quantum mechanical–free energy method with a cratic term to the S_N2

methyl cation transfer catalyzed by catechol O-methyltransferase and obtained good agreement with experiment.

CITRATE SYNTHASE   This system has also been studied by QM/MM methods by two groups using different approaches: potential energy profiles with AM1 and MP2/6-31G* for the quantum mechanical subsystem (98, 220, 221) and quantum mechanical–free energy with restrained electrostatic potential charges from HF/6-31 + G* calculations (163, 167).

HUMAN IMMUNODEFICIENCY VIRUS TYPE-1 (HIV-1) PROTEASE   Liu et al. (222) used link-atom PM3/GROMOS87 calculations in molecular dynamics simulations to calculate a PMF as a function of the making C-O bond distance.

OROTIDINE 5′-MONOPHOSPHATE DECARBOXYLASE (ODCase)   ODCase is involved in the last step of pyrimidine biosynthesis, which catalyzes the decarboxylation of orotidine 5′-monophosphate at a remarkable acceleration rate of 17 orders of magnitude over the uncatalyzed aqueous process. ODCase has been extensively studied both experimentally and computationally. In a joint X-ray crystallographic and computational study, Wu et al. (223) solved the structure of the apo enzyme and the structure complexed with a transition state analog and proposed a mechanism on the basis of free energy calculations of the reaction profile using a combined AM1/CHARMM potential. The computed $\Delta G^{\neq}$ of 37.2 and 14.8 kcal/mol for the uncatalyzed and catalyzed reactions were in excellent agreement with the corresponding experimental values (38.5 and 15.2 kcal/mol, respectively). Wu et al. analyzed the free energy of transfer for the reactive part, orotate ion, from aqueous solution into the enzyme active site using free energy perturbation theory (75, 76) and found that orotate is destabilized by 17.8 kcal/mol owing to electrostatic stress from an Asp residue and a change of the polar aqueous environment to a largely hydrophobic binding pocket (223) surrounding the orotate ion. The reduction in free energy of activation by ODCase was attributed to reactant destabilization, an idea originally proposed by Jencks (224). The destabilization effect is compensated by binding contributions from interactions with the rest of the ribose and phosphate groups of the substrate, which form extended hydrogen bonding and ion-pair interactions with the enzyme.

Warshel and coworkers, on the other hand, carried out a calculation using an EVB potential and suggested that transition state stabilization, rather than reactant destabilization, is responsible for the enormous rate enhancement of 23 kcal/mol by ODCase (225, 226). They interpreted the catalytic enhancement as due to the dipolar environment of the enzyme active site being preorganized such that there is a lower reorganization penalty for the enzymatic reaction than the aqueous one (225). Although the authors did not compute reorganization energy for this reaction and the concept of preorganized dipoles of the enzyme environment may be reasonable to account for transition state stabilization in some enzymes, the application of this explanation to the ODCase reaction neglects the effect of

conformational changes of key residues in ODCase's active site (see Figure 11 in Reference 225). To make this argument work for ODCase, the residue Lys72 has to be deleted from the enzyme and included as part of the substrate. However, it is not clear if this choice of reference state is reasonable for comparison with the reaction catalyzed under physiological conditions by the real enzyme.

PARA-HYDROXY BONZOATE HYDROXYLASE   The 3-hydroxylation of *p*-hydroxy benzoate is catalyzed by para-hydroxy bonzoate hydroxylase, with the chemical step being electrophilic aromatic attack of a C4a-peroxyflavin intermediate formed from the cofactor. Billeter et al. (227) carried out studies with a 102- or 103-atom AM1 subsystem and 6902 GROMOS96 molecular mechanical atoms. The QM/MM interactions were treated by either the mechanical embedding model or the electronic embedding model (228), and free energy profiles were calculated as functions of the making bond distance. They also optimized a transition state structure in the presence of enzyme.

PROTEIN TYROSINE PHOSPHATASE   Alhambra et al. (100) carried out free energy calculations and obtained the PMF for the reaction in a low-molecular-weight protein tyrosine phosphatase. They attributed the lowering of the free energy of activation to Walden-inversion enforced transition state stabilization. The protein tyrosine phosphatase reaction has also been investigated by Aqvist and coworkers using an EVB model (229). They found that a protonated Asp129 residue is favored in the catalytic step, which was used in the study by Alhambra et al. (100).

SUBTILISIN   Colombo et al. (230, 231) used classical molecular dynamics with free energy perturbation to study the enantioselectivity of the serine protease subtilisin in water, dimethylformamide, and hexane. They used the PM3 and MNDO quantum mechanical methods and the AMBER force field for the enzyme and substrate, the OPLS force field for organic solvents, and the TIP3P force field for water.

TRIOSE PHOSPHATE ISOMERASE   Studies (207) involving quantized vibrations are summarized above. There have also been studies with quantal electronic structure and classical nuclear motion. First, Karplus and coworkers used a QM/MM method to determine the potential energy along a reaction path and to provide a decomposition of the energy lowering into contributions from specific residues (232, 233). Later, Cui et al. (234) used a self-consistent-charge density-functional tight-binding quantum mechanical (235) subsystem or an AM1 or AM1-SRP quantum mechanical subsystem with a CHARMM molecular mechanical subsystem and optimized the active site structure with a fixed secondary zone.

Zhang et al. (169) also studied the triose phosphate isomerase reaction using QM/MM methods. They used an HF/3-21G description of a 37-atom quantum mechanical system joined by the pseudobond approach to a 6014-atom molecular mechanical subsystem described by the AMBER and TIP3P force fields. They first optimized a 3008-atom subsystem reactant geometry and then calculated a

forward reaction path all the way to products by a series of restrained minimizations along a distinguished coordinate. They then followed the reverse path back from the products to reactants, obtaining agreement of the potential energy curves within 1 kcal/mol. Then, using the forward reaction path, they used the quantum mechanical–free energy method to obtain the change in free energy of interaction of the quantum mechanical and molecular mechanical subsystems as a function of the reaction coordinate.

Quantum Treatments of Electronic Structure Without Statistical Mechanics

Quantum mechanical electronic structure calculations for an active site in the field of the enzyme environment can be a powerful technique for elucidating the factors underlying enzyme catalysis even when statistical averaging is not employed, provided one proceeds carefully and cautiously and uses good judgment. In fact, this approach has already become so powerful that the amount of work being carried out has exploded, and a complete summary would require more pages than have been allotted for this review. Because it is a very exciting area, though, we summarize selected applications from various groups to illustrate the state of the art and the variety of approaches employed. The following paragraphs are in alphabetical order of enzyme. [Calculations without explicit enzymes are not included, but some of these were reviewed recently (236, 237).]

ALDOSE REDUCTASE   Two studies were carried out using link-atom QM/MM to elucidate the mechanism of the reduction of D-glyceraldehyde by aldose reductase. Lee et al. (238) optimized the geometry of active site residues and constructed reaction paths and reduced-dimensionality potential surfaces. Várnai et al. (239) examined a chain of points on hypothetical proton transfer and hydride transfer reaction paths.

BACTERIORHODOPSIN   Ben-Nun et al. (240) applied the full multiple spawning wave packet dynamics method to study the coupled-electronic-state all-*trans* → 13-*cis* photoisomerization of retinal in bacteriorhodopsin. Their multi-state potential function was an electronically diabatic one with molecular mechanical diagonal elements and constant off-diagonal elements. Rajamani & Gao carried out molecular dynamics simulation of bacteriorhodopsin in a lipid bilayer and the protonated Schiff base in solution using combined AM1/CHARMM and configuration interaction with single excitations/3-21G/CHARMM potentials to compute the opsin shift of bacteriorhodopsin (241). The ensemble-averaged opsin shift of 4200 cm^{-1} without dispersion contributions is in reasonable agreement with the experimental value of 5100 cm^{-1}. When dispersion effects are included, the estimated opsin shift is 5200 cm^{-1}.

CARBONIC ANHYDRASE   Studies (146) involving quantized vibrations are summarized above. Toba et al. (242) investigated carbonic anhydrase using a three-stage

approach. First they used QM/MM calculations with a PM3 quantum mechanical subsystem to partially optimize a reactant geometry. At this geometry they used an MNDO quantum mechanical treatment to calculate partial atomic charges by electrostatic potential fitting. These charges were then used with the AMBER force field for classical molecular dynamics simulations.

CHORISMATE MUTASE   The transformation of chorismate to prephenate by chorismate mutase has been studied independently by several groups using QM/MM. Lyne et al. (243) carried out simulations to study the origin of the catalytic effect. One study (244) focused on comparative evaluation of methodological choices (with quantum mechanical partial atomic charges from electrostatic fitting of a B3LYP/6-31G* treatment of 24 atoms in the environment of 4117 MM atoms) and another (245, 246) (based on 24 AM1 atoms and 6245 CHARMM and TIP3P atoms) focused on the origin of catalytic efficiency. We have also carried out free energy perturbation-VTST/MT calculations to estimate KIEs using an AM1-SRP potential for the chorismate reaction (C. Alhambra & J. Gao, unpublished manuscript).

COLD SHOCK PROTEIN A   Merz and coworkers (62, 63) carried out PM3 quantum mechanical calculations on selected geometries of the entire cold shock protein A in the presence of water. This allowed them to study charge transfer from the protein to water, which was found to be nonnegligible. This raises important questions about the location of QM/MM boundaries because current QM/MM algorithms do not allow charge transfer across the boundary.

CYTIDINE DEAMINASE   Lewis et al. (66, 67) applied PM3 quantum mechanical methods to optimize geometries of a 1330-atom subsystem of cytidine aminase with the active site occupied by cytidine, by a transition state analog, or by uridine (the product). The Zn-S distance at the transition state is largest for the transition state analog.

DIHYDROFOLATE REDUCTASE   Dynamics calculations (21) on dihydrofolate reductase are discussed above. Gready and coworkers (69, 248–250) carried out an interesting series of studies that led to a comparison of QM/MM calculations with quantum mechanical electronic structure calculations on the whole enzyme-substrate system. The quantum mechanical level for the comparison was PM3, and the molecular mechanical subsystem was treated by AMBER94 and TIP3P force fields. They discussed the polarization of the quantum mechanical subsystem by the molecular mechanical one in light of these results, warning against possible pitfalls in the QM/MM calculations, which were 500 times less expensive than the fully quantum mechanical calculations.

ELASTASE   Topf et al. (251) reported link-atom QM/MM energy minimizations on three stationary points along the deacylation step in the elastase reaction. A total

of 49 atoms were treated by quantum mechanics using HF/3-21G and HF/6-31G*, and 12,010 atoms were treated molecular mechanically by CHARMM and TIP3P.

ENOLASE   Dynamics calculations (52) on the enolase reaction are discussed above. More recently Liu et al. (252) have carried out QM/MM calculations of free energy profiles as functions of distance along a restrained-optimization reaction path. They used the pseudobond approach to the QM/MM interface with HF/3-21G and B3LYP/6-31G* quantum mechanical calculations.

GALACTOSE OXIDASE   Röthlisberger et al. (253) applied QM/MM calculations to the H abstraction step catalyzed by galactose oxidase. The quantum region of $\sim$70 atoms was treated by the Becke-Lee-Yang-Parr density functional with a plane wave basis (80 Ry cutoff), and the molecular mechanical region of $\sim$16,000 atoms was treated by CHARMM. They used the scaled-position link-atom method for linking quantum mechanics to molecular mechanics. They optimized structures by energy minimization to serve as typical thermally accessible configurations for further analysis.

HALOALKANE DEHALOGENASE   Lau et al. (254) used QM/MM calculations to study the S_N2 displacement of chloride from 1,2-dichloroethane catalyzed by haloalkane dehalogenase. They used AM1-SRP for the quantum mechanical subsystem (15 atoms) and a combination of CHARMM parameters and MM-SRP parameters optimized for this system for the molecular mechanical subsystem (4237 atoms). The conclusions were based on a two-dimensional grid of energies for two choices of the other coordinates.

HIV-1 PROLEASE   A free energy calculation on this system is mentioned above (222). Chatfield et al. used an ab initio QM/MM approach with CHARMM for the MM part to determine a minimum energy path for the reaction in the enzyme (255, 256). Trylska et al. (257) presented a parameterization of a 23×23 approximate valence bond description of the complete enzymatic reaction catalyzed by HIV-1 protease.

HYDROGENASE   Amara et al. (258) used a B3LYP/effective core potential treatment of a 30-atom quantum subsystem joined by link atoms to a CHARMM subsystem of 10,000 atoms in residues within 27 Å of the active site to optimize reactant structures of Ni-Fe hydrogenase.

β-LACTAMASES   Both class A (259–261) and class B (262) β-lactamases have been studied with QM/MM, in both cases employing energy minimizations, either with a fixed molecular mechanical region or with the molecular mechanical region also energy optimized (261).

LACTATE DEHYDROGENASE   The lactate dehydrogenase system presents an informative case history in which two seemingly similar QM/MM calculations led to

different mechanistic conclusions about the order of proton transfer and hydride transfer and the degree of synchronicity of these steps (263–266). Furthermore, transition state optimizations starting at various points lead to different structures. Although this result is not surprising in itself (this is one reason why reliable dynamics procedures for enzyme reactions should be based on an ensemble of transition structures such as those in the highest window of a free energy profile), in this case the variation in disposition of active site residues was very large (265). Poetically, the authors commented, "depending upon how a gentle breeze may gust at the crucial moment, a raindrop falling on the Andes may flow either to the Atlantic or the Pacific. So it is with geometry optimization in a large and flexible system" (266). Although the classification of transition structures into the two mechanisms was not as sensitive to initial conditions of the optimization, the energetics of the two mechanisms are similar enough that it will be hard to tell which is preferred by nature.

MALATE DEHYDROGENASE Bash and coworkers (267, 268) calculated two-dimensional energy surfaces for the conversion of malate to oxaloacetate by malate dehydrogenase.

MANDELATE RACEMATE A QM/MM study of potential energies for the racemization of vinylglycolate catalyzed by mandelate racemate found three competitive parallel mechanisms (269). The authors commented that an exploration of the PES to locate possibly unexpected critical points should precede the choice of reaction coordinate for calculating a free energy of activation profile.

PAPAIN Han et al. (270) scanned the PES for proton transfer catalyzed by papain with HF and B3LYP in the active site surrounded by fixed enzymes with AMBER charges. Harrison et al. (271) used AM1/CHARMM to find a transition structure for amide hydrolysis by papain.

PARA-HYDROXY BONZOATE HYDROXYLASE Free energy profiles (227) are discussed above. Whereas those calculations indicated a free energy of activation of 12 kcal/mol, energy optimizations by the same authors with the same QM/MM Hamiltonian yielded 21 kcal/mol, showing the danger of the latter type of calculation for predicting rate constants. Using the difference of two bond lengths as a reaction coordinate, Ridder et al. (272–274) used link-atom QM/MM with AM1 and CHARMM22 for the subsystems to find a distinguished-coordinate reaction path, which involves optimizing other coordinates for fixed values of the reaction coordinate. This allowed them to estimate a barrier height and study the role of the cofactor and active site amino acids.

PHENOL HYDROXYLASE Ridder et al. (275) used AM1/CHARMM to calculate a two-dimensional energy surface for hydroxylation of phenol by phenol hydroxylase. Starting at the transition structure so identified, they performed energy

minimizations for a series of substituted phenols to examine the variation in catalytic activity.

PLA$_2$ Dynamics calculations (55) on PLA$_2$ are discussed above. Hillier and co-workers (276, 277) applied the QM/MM method to the transition state for amide hydrolysis by PLA$_2$. Schürer et al. (278) also studied PLA$_2$, a coenzyme that hydrolyzes an ester bond of L-glycerophospholipids. They treated an active-site model of 156 atoms with PM3 and surrounded this with a fixed molecular mechanical region described by the PARAM94 force field of AMBER. Coulomb interactions between the quantum mechanical subsystem and the molecular mechanical region were modeled with dielectric constant 4, but this was varied from 1 to 78 to study the effect of this assumption on the calculated potential energy profiles.

PROTEIN TYROSINE PHOSPHATASE   Free energy calculations are mentioned above (100, 229). Hart et al. (279, 280) computed the transition structure using AM1/MM and PM3/MM potentials and predicted a dissociative mechanism for the dephosphorylation reaction in protein tyrosine phosphatase.

RUBISCO   Moliner et al. (281) calculated AM1/CHARMM transition state structures for the carboxylation of D-ribulose-1,5-diphosphate catalyzed by rubisco.

THERMOLYSIN   Antonczak et al. (282, 283) studied two mechanisms for the hydrolysis of formamide and a tripeptide by the Zn protease thermolysin. They used AM1 with the LSCF formalism with parameters extracted from a model system, and they used the AMBER force field for the molecular mechanical part. They optimized reactant and transition state structures of the quantum mechanical subsystem with the fixed molecular mechanical subsystem.

THYMIDINE PHOSPHORYLASE   Burton et al. (280) used a PM3/AMBER hybrid with a charge redistribution algorithm for minimizing adverse effects from link atoms to calculate potential energy barriers for phosphorolysis in thymidine phosphorylase. They optimized reactant and transition state structures of the quantum mechanical subsystem with fixed molecular mechanical regions and then energy minimized the molecular mechanical region with a fixed quantum mechanical subsystem to learn about enzyme structure changes during the reaction. They also explored the effects of moving residues from the molecular mechanical region into the quantum mechanical subsystem.

CONCLUDING REMARKS

In this article we review methods for enzyme kinetics modeling and applications that incorporate quantum mechanical effects in the computation. Three aspects are emphasized, namely the treatment of the electronic structure of atoms involved in the chemical process in an enzyme, the incorporation of quantum vibrational

free energies into the calculation of the potential of mean force, and the use of multidimensional tunneling methods for estimating the transmission coefficient. It is evident from the applications we have summarized here that the incorporation of quantum mechanical effects is essential for enzyme kinetics simulations, and the computational accuracy has been tremendously increased in the past several years in comparison with experiment. These computational approaches provide insights and help interpret experimental data such as kinetic isotope effects and the significance of such factors as dynamics and tunneling in enzymatic processes. Still, there is much to improve in computational techniques, sampling, and time and length scales relevant to physiological conditions.

Visit the Annual Reviews home page at www.annualreviews.org

LITERATURE CITED

1. Wigner EP. 1938. *Trans. Faraday Soc.* 34:29–41

2. Glasstone S, Laidler KJ, Eyring H. 1941. *The Theory of Rate Processes*. New York: McGraw-Hill

3. Keck JC. 1967. *Adv. Chem. Phys.* 13:85–121

4. Anderson JB. 1973. *J. Chem. Phys.* 58:4684–92

5. Truhlar DG, Garrett BC. 1980. *Acc. Chem. Res.* 13:440–48

6. Pechukas P. 1981. *Annu. Rev. Phys. Chem.* 32:159–72

7. Pechukas P. 1982. *Ber. Bunsenges. Phys. Chem.* 86:372–78

8. Truhlar DG, Hase WL, Hynes JT. 1983. *J. Phys. Chem.* 87:2664–82. Erratum. 1983. *J. Phys. Chem.* 87:5523

9. Truhlar DG, Garrett BC. 1984. *Annu. Rev. Phys. Chem.* 35:159–89

10. Tucker SC, Truhlar DG. 1989. In *New Theoretical Concepts for Understanding Organic Reactions*, ed. J Bertran, IG Csizmadia, pp. 291–346. Dordrecht, The Netherlands: Kluwer

11. Truhlar DG, Garrett BC, Klippenstein SJ. 1996. *J. Phys. Chem.* 100:12771–800

12. Garrett BC, Truhlar DG. 1998. In *Encyclopedia of Computational Chemistry*, ed. PvR Schleyer, NL Allinger, T Clark, J Gasteiger, PA Kollman, HF Schaefer III. 5:3094–104. Chichester, UK: Wiley

13. Grimmelmann EK, Tully JC, Helfand E. 1981. *J. Chem. Phys.* 74:5300–10

14. Keck JC. 1962. *Discuss. Faraday Soc.* 33:173–82

15. Chandler D. 1978. *J. Chem. Phys.* 68:2959–70

16. Montgomery JA Jr, Chandler D, Berne BJ. 1979. *J. Chem. Phys.* 70:4056–66

17. Grote RF, Hynes JT. 1980. *J. Chem. Phys.* 73:2715–32

18. Northrup SH, Pear MR, Lee CY, McCammon JA, Karplus M. 1982. *Proc. Natl. Acad. Sci. USA* 79:4035–39

19. Bergsma JP, Gertner BJ, Wilson KR, Hynes JT. 1987. *J. Chem. Phys.* 86:1356–76

20. Hwang JK, King G, Creighton S, Warshel A. 1988. *J. Am. Chem. Soc.* 110:5297–311

21. Neria E, Karplus M. 1997. *Chem. Phys. Lett.* 267:26–30

22. Miller WH. 1996. In *Dynamics of Molecules and Chemical Reactions*, ed. RE Wyatt, JZH Zhang, pp. 387–410. New York: Marcel Dekker

23. Natanson GA, Garrett BC, Truong TN, Joseph T, Truhlar DG. 1991. *J. Chem. Phys.* 94:7875–92

24. Gao J. 1996. *Acc. Chem. Res.* 29:298–305

25. Marcus RA. 1956. *J. Chem. Phys.* 24:966–78

26. Warshel A. 1982. *J. Phys. Chem.* 86: 2218–24

27. Schenter GK, Garrett BC, Truhlar DG. 2001. *J. Phys. Chem. B* 105:9672–85

28. Mo Y, Gao J. 2000. *J. Phys. Chem. A* 104: 3012–20

29. Garrett BC. 2000. *Theor. Chem. Acc.* 103: 200–4

30. Villa J, Truhlar DG. 1997. *Theor. Chem. Acc.* 97:317–23

31. Boyd RK. 1977. *Chem. Rev.* 77:93–119

32. Dellago C, Bolhuis PG, Chandler D. 1998. *J. Chem. Phys.* 108:9236–45

33. Dellago C, Bolhuis PG, Csajka FS, Chandler D. 1998. *J. Chem. Phys.* 108: 1964–77

34. Dellago C, Bolhuis PG, Chandler D. 1999. *J. Chem. Phys.* 110:6617–25

35. Valleau JP, Torrie GM. 1977. In *Modern Theoretical Chemistry*, ed. BJ Berne, 5:169–94. New York: Plenum

36. Zwanzig R. 1954. *J. Chem. Phys.* 22: 1420–26

37. Brooks CL III, Karplus M, Pettitt BM. 1988. *Adv. Chem. Phys.* 71:1–259

38. MacKerell AD Jr, Wiorkiewicz-Kuczera J, Karplus M. 1995. *J. Am. Chem. Soc.* 117:11946–75

39. Cornell WD, Cieplak P, Bayly CI, Gould IR, Merz KM Jr, et al. 1995. *J. Am. Chem. Soc.* 117:5179–97

40. MacKerell AD Jr, Bashford D, Bellott M, Dunbrack RL, Evanseck JD, et al. 1998. *J. Phys. Chem. B* 102:3586–616

41. Jorgensen WL, Tirado-Rives J. 1988. *J. Am. Chem. Soc.* 110:1657–66

42. Wang W, Donini O, Reyes CM, Kollman PA. 2001. *Annu. Rev. Biophys. Biomol. Struct.* 30:211–43

43. Johnston HS. 1966. *Gas Phase Reaction Rate Theory*. New York: Ronald

44. Bennett CH. 1977. *ACS Symp. Ser.* 46:63–97

45. Smith IWM. 1981. *J. Chem. Soc. Faraday Trans. II* 77:747–59

46. Truhlar DG, Garrett BC. 1987. *Faraday Discuss. Chem. Soc.* 84:464

47. Schenter GK, Messina M, Garrett BC. 1993. *J. Chem. Phys.* 99:1674–84

48. Alhambra C, Corchado JC, Sanchez ML, Garcia-Viloca M, Gao J, Truhlar DG. 2001. *J. Phys. Chem. B* 105:11326–40

49. Billeter SR, Webb SP, Iordanov T, Agarwal PK, Hammes-Schiffer S. 2001. *J. Chem. Phys.* 114:6925–36

50. Cramer CJ, Truhlar DG. 1999. *Chem. Rev.* 99:2161–200

51. Burton NA, Harrison MJ, Hillier IH, Jones NR, Tantanak D, Vincent MA. 1999. *ACS Symp. Ser.* 721:401–10

52. Alhambra C, Gao J, Corchado JC, Villa J, Truhlar DG. 1999. *J. Am. Chem. Soc.* 121:2253–58

53. Thomas A, Jourand D, Bret C, Amara P, Field MJ. 1999. *J. Am. Chem. Soc.* 121: 9693–702

54. Alhambra C, Corchado JC, Sanchez ML, Gao J, Truhlar DG. 2000. *J. Am. Chem. Soc.* 122:8197–203

55. Bala P, Grochowski P, Nowinski K, Lesyng B, McCammon JA. 2000. *Biophys. J.* 79:1253–62

56. Nicoll RM, Hindle SA, MacKenzie G, Hillier IH, Burton NA. 2001. *Theor. Chem. Acc.* 106:105–12

57. Faulder PF, Tresadern G, Chohan KK, Scrutton NS, Sutcliffe MJ, et al. 2001. *J. Am. Chem. Soc.* 123:8604–5

58. Alhambra C, Sanchez ML, Corchado J, Gao J, Truhlar DG. 2001. *Chem. Phys. Lett.* 347:512–18; Erratum. In press

59. Truhlar DG, Gao J, Alhambra C, Garcia-Viloca M, Corchado J, et al. 2002. *Acc. Chem. Res.* In press

60. Dixon SL, Merz KM Jr. 1996. *J. Chem. Phys.* 104:6643–49

61. Van der Vaart A, Merz KM Jr. 1999. *J. Phys. Chem. A.* 103:3321–29

62. Nadig G, Van Zant LC, Dixon SL, Merz KM Jr. 1999. *ACS Symp. Ser.* 721:439–47

63. Van der Vaart A, Merz KM Jr. 1999. *J. Am. Chem. Soc.* 121:9182–90

64. Lee T-S, York DM, Yang WT. 1996. *J. Chem. Phys.* 105:2744–50

65. York DM, Lee T-S, Yang WT. 1998. *Phys. Rev. Lett.* 80:5011–14

66. Lewis JP, Carter CW Jr, Hermans J, Pan W, Lee T-S, Yang WT. 1998. *J. Am. Chem. Soc.* 120:5407–10

67. Lewis JP, Liu SB, Lee T-S, Yang WT. 1999. *J. Comput. Phys.* 151:242–63

68. Stewart JJP. 1997. *Theochem* 401:195–205

69. Titmuss SJ, Cummins PL, Bliznyuk AA, Rendell AP, Gready JE. 2000. *Chem. Phys. Lett.* 320:169–76

70. Gao J, Thompson MA. 1998. *Combined Quantum Mechanical and Molecular Mechanical Methods*. Washington, DC: Am. Chem. Soc.

71. Warshel A, Levitt M. 1976. *J. Mol. Biol.* 103:227–49

72. Singh UC, Kollman PA. 1986. *J. Comput. Chem.* 7:718–30

73. Tapia O, Lluch JM, Cardenas R, Andres J. 1989. *J. Am. Chem. Soc.* 111:829–35

74. Field MJ, Bash PA, Karplus M. 1990. *J. Comput. Chem.* 11:700–33

75. Gao J. 1992. *J. Phys. Chem.* 96:537–40

76. Gao J, Xia XF. 1992. *Science* 258:631–35

77. Stanton RV, Hartsough DS, Merz KM Jr. 1993. *J. Phys. Chem.* 97:11868–70

78. Gao J. 1994. *ACS Symp. Ser.* 569:8–21

79. Gao J. 1994. *J. Am. Chem. Soc.* 116:9324–28

80. Gao J. 1995. In *Reviews in Computational Chemistry*, ed. KB Lipkowitz, DB Boyd, 7:119–85. New York: VCH

81. Freindorf M, Gao J. 1996. *J. Comput. Chem.* 17:386–95

82. Gao J. 1997. *J. Comput. Chem.* 18:1062–971

83. Alhambra C, Byun K, Gao J. 1998. *ACS Symp. Ser.* 712:35–49

84. Warshel A, Karplus M. 1972. *J. Am. Chem. Soc.* 94:5612–25

85. Gao J, Furlani TR. 1995. *IEEE Comput. Sci. Eng.* 2(3):24–33

86. Monard G, Merz KM Jr. 1999. *Acc. Chem. Res.* 32:904–11

87. Pople JA, Santry DP, Segal GA. 1965. *J. Chem. Phys.* 43:S129–35

88. Dewar MJS, Zoebisch EG, Healy EF, Stewart JJP. 1985. *J. Am. Chem. Soc.* 107:3902–9

89. Stewart JJP. 1990. *J. Comput.-Aided Mol. Des.* 4:1–105

90. Dewar MJS, Thiel W. 1977. *J. Am. Chem. Soc.* 99:4899–907

91. Hehre WJ, Radom L, Schleyer PvR, Pople JA. 1986. *Ab Initio Molecular Orbital Theory*. New York: Wiley

92. Becke AD. 1988. *Phys. Rev. A* 38:3098–100

93. Lee CT, Yang WT, Parr RG. 1988. *Phys. Rev. B* 37:785–89

94. Stephens PJ, Devlin FJ, Chabalowski CF, Frisch MJ. 1994. *J. Phys. Chem.* 98:11623–27

95. Krauss M, Stevens WJ. 1984. *Annu. Rev. Phys. Chem.* 35:357–85

96. Car R, Parrinello M. 1985. *Phys. Rev. Lett.* 55:2471–74

97. Aqvist J, Warshel A. 1993. *Chem. Rev.* 93:2523–44

98. Mulholland AJ. 2001. *Theor. Comput. Chem.* 9:597–653

99. Gao J, Amara P, Alhambra C, Field MJ. 1998. *J. Phys. Chem. A* 102:4714–21

100. Alhambra C, Wu L, Zhang Z-Y, Gao J. 1998. *J. Am. Chem. Soc.* 120:3858–66

101. Reuter N, Dejaegere A, Maigret B, Karplus M. 2000. *J. Phys. Chem. A* 104:1720–35

102. Eichinger M, Tavan P, Hutter J, Parrinello M. 1999. *J. Chem. Phys.* 110:10452–67

102a. Ostlund NS. Personal communication. See also: 1994. *HyperChem, Getting Started*, pp. 195–96 Hypercube, Inc.

103. Zhang YK, Lee T-S, Yang WT. 1999. *J. Chem. Phys.* 110:46–54

104. Thery V, Rinaldi D, Rivail JL, Maigret B, Ferenczy GG. 1994. *J. Comput. Chem.* 15:269–82

105. Monard G, Loos M, Thery V, Baka K, Rivail J-L. 1996. *Int. J. Quantum Chem.* 58:153–59

106. Assfeld X, Rivail J-L. 1996. *Chem. Phys. Lett.* 263:100–6

107. Assfeld X, Ferre N, Rivail J-L. 1998. *ACS Symp. Ser.* 712:234–49

108. Ferre N, Assfeld X, Rivail J-L. 2002. Preprint. In press

109. Amara P, Field MJ, Alhambra C, Gao J. 2000. *Theor. Chem. Acc.* 104:336–43

110. Murphy RB, Philipp DM, Friesner RA. 2000. *Chem. Phys. Lett.* 321:113–20

111. Antes I, Thiel W. 1998. *ACS Symp. Ser.* 712:50–65

112. Antes I, Thiel W. 1999. *J. Phys. Chem.* 103:9290–95

113. Bersuker IB, Leong MK, Boggs JE, Pearlman RS. 1998. *ACS Symp. Ser.* 712:66–91

114. Gonzalez-Lafont A, Truong TN, Truhlar DG. 1991. *J. Phys. Chem.* 95:4618–27

115. Rossi I, Truhlar DG. 1995. *Chem. Phys. Lett.* 233:231–36

116. Bash PA, Ho L, MacKerell AD Jr, Levine D, Hallstrom P. 1996. *Proc. Natl. Acad. Sci. USA* 93:3698–703

117. Truhlar DG, Parr CA. 1971. *J. Phys. Chem.* 75:1844–60

118. Gao J. 1993. *J. Am. Chem. Soc.* 115:2930–35

119. Gao J, Xia X. 1994. *ACS Symp. Ser.* 568:212–28

120. Gao J. 1995. *J. Am. Chem. Soc.* 117:8600–7

121. Sehgal A, Shao L, Gao J. 1995. *J. Am. Chem. Soc.* 117:11337–40

122. Byun K, Mo Y, Gao J. 2001. *J. Am. Chem. Soc.* 123:3974–79

123. Maseras F, Morokuma K. 1995. *J. Comput. Chem.* 16:1170–79

124. Gao J. 1994. *Proc. Indiana Acad. Sci.* 106:507–19

125. Warshel A. 1991. *Computer Modeling of Chemical Reactions in Enzymes and Solutions.* New York: Wiley

126. Coulson CA, Danielson U. 1954. *Ark. Fys.* 8:245–55

127. Warshel A, Weiss RM. 1980. *J. Am. Chem. Soc.* 102:6218–26

128. Warshel A, Weiss RM. 1981. *Ann. NY Acad. Sci.* 367:370–82

129. Warshel A, Russell ST, Weiss RM. 1982. *Stud. Org. Chem.* 10:267–74

130. Warshel A, Russell S. 1986. *J. Am. Chem. Soc.* 108:6569–79

131. Aqvist J, Fothergill M, Warshel A. 1993. *J. Am. Chem. Soc.* 115:631–35

132. Aqvist J. 1997. *Underst. Chem. React.* 19:341–62

133. Feierberg I, Luzhkov V, Aqvist J. 2000. *J. Biol. Chem.* 275:22657–62

134. Agarwal PK, Webb SP, Hammes-Schiffer S. 2000. *J. Am. Chem. Soc.* 122:4803–12

135. Villà J, Warshel A. 2001. *J. Phys. Chem. B* 105:7887–907

136. Mo Y, Gao J. 2000. *J. Comput. Chem.* 21:1458–69

137. Mo Y, Peyerimhoff SD. 1998. *J. Chem. Phys.* 109:1687–97

138. Mo Y, Zhang YQ, Gao J. 1999. *J. Am. Chem. Soc.* 121:5737–42

139. Schmitt UW, Voth GA. 1998. *J. Phys. Chem. B* 102:5547–51

140. Schmitt UW, Voth GA. 1999. *J. Chem. Phys.* 111:9361–81

141. Kim Y, Corchado JC, Villa J, Xing J, Truhlar DG. 2000. *J. Chem. Phys.* 112:2718–35

142. Albu TV, Corchado JC, Truhlar DG. 2001. *J. Phys. Chem. A* 105:8465–87

143. Field MJ. 1993. In *Computer Simulation of Biomolecular Systems*, ed. WF van Gunsteren, PK Weiner, AJ Wilkinson, 2:82–123. Leiden, The Netherlands: ESCOM

144. Espinosa-Garcia J, Corchado JC, Truhlar DG. 1997. *J. Am. Chem. Soc.* 119:9891–96

145. Garcia-Viloca M, Alhambra C, Truhlar DG, Gao J. 2001. *J. Chem. Phys.* 114:9953–58

146. Hwang J-K, Warshel A. 1996. *J. Am. Chem. Soc.* 118:11745–51

147. Feynman RP, Hibbs AR. 1965. *Quantum Mechanics and Path Integrals.* New York: McGraw-Hill

148. Gillan MJ. 1988. *Philos. Mag. A* 58:257–83

149. Voth GA, Chandler D, Miller WH. 1989. *J. Chem. Phys.* 91:7749–60

150. Messina M, Schenter GK, Garrett BC. 1993. *J. Chem. Phys.* 98:8525–36

151. Cao J, Voth GA. 1994. *J. Chem. Phys.* 101:6184–92

152. Lobaugh J, Voth GA. 1992. *Chem. Phys. Lett.* 198:311–15

153. Hwang JK, Warshel A. 1993. *J. Phys. Chem.* 97:10053–58

154. Jang S, Voth GA. 2000. *J. Chem. Phys.* 112:8747–57. Erratum. 2001. *J. Chem. Phys.* 114:1944

155. Makarov DE, Topaler M. 1995. *Phys. Rev. E* 52:178–88

156. Messina M, Schenter GK, Garrett BC. 1995. *J. Chem. Phys.* 103:3430–35

157. Mills G, Schenter GK, Makarov DE, Jonsson H. 1997. *Chem. Phys. Lett.* 278:91–96

158. Jang S, Schwieters CD, Voth GA. 1999. *J. Phys. Chem. A* 103:9527–38

158a. Mielke SL, Truhlar DG. 2001. *J. Chem. Phys.* 115:652–62

159. Tuckerman ME, Marx D. 2001. *Phys. Rev. Lett.* 86:4946–49

160. Hammes-Schiffer S. 1998. *J. Phys. Chem. A* 102:10443–54

161. Webb SP, Hammes-Schiffer S. 2000. *J. Chem. Phys.* 113:5214–27

162. Stanton RV, Peraekylae M, Bakowies D, Kollman PA. 1998. *J. Am. Chem. Soc.* 120:3448–57

163. Kuhn B, Kollman PA. 2000. *J. Am. Chem. Soc.* 122:2586–96

164. Lee TS, Massova I, Kuhn B, Kollman PA. 2000. *J. Chem. Soc. Perkin Trans. II* 3:409–15

165. Donini O, Darden T, Kollman PA. 2000. *J. Am. Chem. Soc.* 122:12270–80

166. Peraekylae M, Kollman PA. 2000. *J. Am. Chem. Soc.* 122:3436–44

167. Kollman PA, Kuhn B, Donini O, Peraekylae M, Stanton R, Bakowies D. 2001. *Acc. Chem. Res.* 34:72–79

168. Chandrasekhar J, Smith SF, Jorgensen WL. 1984. *J. Am. Chem. Soc.* 106:3049–50

169. Zhang YK, Liu HY, Yang WT. 2000. *J. Chem. Phys.* 112:3483–92

170. Bala P, Grochowski P, Lesyng B, McCammon JA. 1996. *J. Phys. Chem.* 100:2535–45

171. Alimi R, Gerber RB, Hammerich AD, Kosloff R, Ratner MA. 1990. *J. Chem. Phys.* 93:6484–90

172. Gerber RB, Alimi R. 1991. *Isr. J. Chem.* 31:383–93

173. Mavri J, Berendsen HJC. 1995. *J. Phys. Chem.* 99:12711–17

174. Berendsen HJC, Mavri J. 1996. *Int. J. Quantum Chem.* 57:975–83

175. Hammes-Schiffer S, Tully JC. 1995. *J. Chem. Phys.* 103:8528–37

176. Tully JC. 1990. *J. Chem. Phys.* 93:1061–71

177. Hammes-Schiffer S, Tully JC. 1994. *J. Chem. Phys.* 101:4657–67

178. Fang J-Y, Hammes-Schiffer S. 1999. *J. Phys. Chem. A* 103:9399–407

179. Lauderdale JG, Truhlar DG. 1986. *J. Chem. Phys.* 84:1843–49

180. Liu YP, Lynch GC, Truong TN, Lu DH, Truhlar DG, Garrett BC. 1993. *J. Am. Chem. Soc.* 115:2408–15

181. Liu YP, Lu DH, Gonzalez-Lafont A, Truhlar DG, Garrett BC. 1993. *J. Am. Chem. Soc.* 115:7806–17

182. Garrett BC, Truhlar DG, Wagner AF, Dunning TH Jr. 1983. *J. Chem. Phys.* 78:4400–13

183. Fernandez-Ramos A, Truhlar DG. 2001. *J. Chem. Phys.* 114:1491–96

184. Garrett BC, Truhlar DG, Grev RS, Magnuson AW. 1980. *J. Phys. Chem.* 84:1730–48

185. Truhlar DG, Isaacson AD, Garrett BC. 1985. In *Theory of Chemical Reaction Dynamics*, ed. M Baer, pp. 65–137. Boca Raton, FL: CRC Press

186. Kreevoy MM, Ostovic D, Truhlar DG, Garrett BC. 1986. *J. Phys. Chem.* 90:3766–74

187. Truhlar DG, Garrett BC. 1987. *J. Chim. Phys.* 84:365–69

188. Truong TN, Lu D-h, Lynch GL, Liu Y-P, Melissas VS, et al. 1993. *Comput. Phys. Commun.* 75:143–59

189. Truhlar DG, Liu Y-P, Schenter GK, Garrett BC. 1994. *J. Phys. Chem.* 98:8396–405

190. Chuang Y-Y, Truhlar DG. 1999. *J. Am. Chem. Soc.* 121:10157–67

191. Schatz GC, Ratner MA. 1993. In *Quantum Mechanics in Chemistry*, pp. 167–72. Englewoods Cliffs, NJ: Prentice-Hall

192. Miller WH. 1974. *Adv. Chem. Phys.* 25:69–177

193. Jasper AW, Hack MD, Truhlar DG. 2001. *J. Chem. Phys.* 115:1804–16

194. Allison TC, Truhlar DG. 1998. In *Modern Methods for Multidimensional Dynamics Computations in Chemistry*, ed. DL Thompson, pp. 618–712. Singapore: World Sci.

195. Pu J, Corchado JC, Truhlar DG. 2001. *J. Chem. Phys.* 115:6266–67

196. Schenter GK, Garrett BC, Truhlar DG. 2001. *J. Phys. Chem. B* 105:9672–85

196a. McRae RP, Schenter GK, Garrett BC, Svetlicic Z, Truhlar DG. 2001. *J. Chem. Phys.* 115:8460–80

197. Hwang JK, Chu ZT, Yadav A, Warshel A. 1991. *J. Phys. Chem.* 95:8445–48

198. Warshel A, Hwang JK. 1992. *Faraday Discuss.* 93:225–38

199. Pawlak J, O'Leary MH, Paneth P. 1999. *ACS Symp. Ser.* 721:462–72

200. Castillo R, Andres J, Moliner V. 1999. *J. Am. Chem. Soc.* 121:12140–47

201. Antoniou D, Schwartz SD. 2001. *J. Phys. Chem. B* 105:5553–58

202. Bahnson BJ, Park DH, Kim K, Plapp BV, Klinman JP. 1993. *Biochemistry* 32:5503–7

203. Bahnson BJ, Klinman JP. 1995. *Methods Enzymol.* 249:373–97

204. Bondi DK, Connor JNL, Garrett BC, Truhlar DG. 1983. *J. Chem. Phys.* 78:5981–89

205. Truhlar DG. 1994. *J. Chem. Soc. Faraday Trans.* 90:1740–43

206. Webb SP, Agarwal PK, Hammes-Schiffer S. 2000. *J. Phys. Chem. B* 104:8884–94

207. Cui Q, Karplus M. 2001. *J. Am. Chem. Soc.* 123:2284–90

208. Brooks HB, Jones LH, Davidson VL. 1993. *Biochemistry* 32:2725–29

209. Basran J, Sutcliffe MJ, Scrutton NS. 1999. *Biochemistry* 38:3218–22

210. Hu H, Liu HY, Shi YY. 1997. *Proteins* 27:545–55

211. Lavie A, Allen KN, Petsko GA, Ringe D. 1994. *Biochemistry* 33:5469–80

212. Allen KN, Lavie A, Glasfeld A, Tanada TN, Gerrity DP, et al. 1994. *Biochemistry* 33:1488–94

213. Bhosale SH, Rao MB, Deshpande VV. 1996. *Microbiol. Rev.* 60:280–300

214. Whitlow M, Howard AJ, Finzel BC, Poulos TL, Winborne E, Gilliland GL. 1991. *Proteins Struct. Funct. Genet.* 9:153–73

215. Jorgensen WL, Chandrasekhar J, Madura JD, Impey RW, Klein ML. 1983. *J. Chem. Phys.* 79:926–35

216. Lee C, Bagdasarian M, Meng M, Zeikus JG. 1990. *J. Biol. Chem.* 265:19082–90

217. Van Tilbeurgh H, Jenkins J, Chiadmi M, Janin J, Wodak SJ, et al. 1992. *Biochemistry* 31:5467–71

218. van Bastelaere PBM, Kersters-Hilderson HLM, Lambeir A-M. 1995. *Biochem. J.* 307:135–42

219. Proust-De Martin F, Dumas R, Field MJ. 2000. *J. Am. Chem. Soc.* 122:7688–97

220. Mulholland AJ, Richards WG. 1999. *ACS Symp. Ser.* 721:448–61

221. Mulholland AJ, Lyne PD, Karplus M. 2000. *J. Am. Chem. Soc.* 122:534–35

222. Liu H, Mueller-Plathe F, van Gunsteren WF. 1996. *J. Mol. Biol.* 261:454–69

223. Wu N, Mo Y, Gao J, Pai EF. 2000. *Proc. Natl. Acad. Sci. USA* 97:2017–22

224. Jencks WP. 1975. *Adv. Enzymol. Relat. Areas Mol. Biol.* 43:219–410

225. Warshel A, Strajbl M, Villa J, Florian J. 2000. *Biochemistry* 39:14728–38

226. Warshel A, Florian J, Strajbl M, Villa J. 2001. *ChemBioChem* 2:109–11

227. Billeter SR, Hanser CFW, Mordasini TZ, Scholten M, Thiel W, van Gunsteren WF. 2001. *Phys. Chem. Chem. Phys.* 3:688–95

228. Bakowies D, Thiel W. 1996. *J. Phys. Chem.* 100:10580–94

229. Hansson T, Nordlund P, Aqvist J. 1997. *J. Mol. Biol.* 265:118–27

230. Columbo G, Ottolina G, Carrea G, Merz KM Jr. 2000. *Chem. Commun.* pp. 559–60

231. Colombo G, Toba S, Merz KM Jr. 1999. *J. Am. Chem. Soc.* 121:3486–93

232. Bash PA, Field MJ, Davenport RC, Petsko GA, Ringe D, Karplus M. 1991. *Biochemistry* 30:5826–32

233. Karplus M, Evanseck JD, Joseph D, Bash PA, Field MJ. 1992. *Faraday Discuss.* 93:239–48

234. Cui Q, Elstner M, Kaxiras E, Frauenheim T, Karplus M. 2001. *J. Phys. Chem. B* 105:569–85

235. Elstner M, Porezag D, Juugnickel G, Elsner J, Haugk M, et al. 1998. *Phys. Rev. B* 58:7260–68

236. Clark T, Gedeck P, Lanig H, Schurer G. 1997. In *Molecular Modeling and Dynamics of Bioinorganic Systems*, ed. L Bauci, P Camba, pp. 307–17. Dordrecht, The Netherlands: Kluwer

237. Siegbahn PEM, Blomberg MRA. 1999. *Annu. Rev. Phys. Chem.* 50:221–49

238. Lee YS, Hodoscek M, Brooks BR, Kador PF. 1998. *Biophys. Chem.* 70:203–16

239. Várnai P, Richards WG, Lyne PD. 1999. *Proteins* 37:218–27

240. Ben-Nun M, Molnar F, Lu H, Phillips JC, Martinez TJ, Schulten K. 1998. *Faraday Discuss.* 110:447–62

241. Rajamani R, Gao J. 2002. *J. Comput. Chem.* 23:96–105

242. Toba S, Colombo G, Merz KM Jr. 1999. *J. Am. Chem. Soc.* 121:2290–302

243. Lyne PD, Mulholland AJ, Richards WG. 1995. *J. Am. Chem. Soc.* 117:11345–50

244. Hall RJ, Hindle SA, Burton NA, Hillier IH. 2000. *J. Comput. Chem.* 21:1433–41

245. Marti S, Andres J, Moliner V, Silla E, Tunon I, et al. 2001. *J. Am. Chem. Soc.* 123:1709–12

246. Marti S, Andres J, Moliner V, Silla E, Tunon I, Bertran J. 2000. *J. Phys. Chem. B* 104:11308–15

247. Deleted in proof

248. Cummins PL, Gready JE. 1998. *ACS Symp. Ser.* 712:250–63

249. Cummins PL, Gready JE. 2000. *J. Phys. Chem. B* 104:4503–10

250. Greatbanks SP, Gready JE, Limaye AC, Rendell AP. 2000. *J. Comput. Chem.* 21:788–811

251. Topf M, Várnai P, Richards WG. 2001. *Theor. Chem. Acc.* 106:146–51

252. Liu H, Zhang Y, Yang W. 2000. *J. Am. Chem. Soc.* 122:6560–70

253. Röthlisberger U, Carloni P, Doclo K, Parrinello M. 2000. *J. Biol. Inorg. Chem.* 5:236–50

254. Lau EY, Kahn K, Bash PA, Bruice TC. 2000. *Proc. Natl. Acad. Sci. USA* 97:9937–42

255. Chatfield DC, Brooks BR. 1995. *J. Am. Chem. Soc.* 117:5561–72

256. Chatfield DC, Eurenius KP, Brooks BR. 1998. *Theochem J. Mol. Struct.* 423:79–92

257. Trylska J, Grochowski P, Geller M. 2001. *Int. J. Quantum Chem.* 82:86–103

258. Amara P, Volbeda A, Fontecilla-Camps JC, Field MJ. 1999. *J. Am. Chem. Soc.* 121:4468–77

259. Pitarch J, Pascual-Ahuir J-L, Silla E, Tunon I, Ruiz-Lopez MF. 1999. *J. Comput. Chem.* 20:1401–11

260. Pitarch J, Pascual-Ahuir J-L, Silla E, Tunon I, Moliner V. 1999. *J. Chem. Soc. Perkin Trans. 2*, pp. 1351–56

261. Pitarch J, Pascual-Ahuir J-L, Silla E, Tunon I. 2000. *J. Chem. Soc. Perkin Trans. 2*, pp. 761–67

262. Suarez D, Merz KM Jr. 2001. *J. Am. Chem. Soc.* 123:7687–90

263. Ranganathan S, Gready JE. 1997. *J. Phys. Chem. B* 101:5614–18

264. Moliner V, Turner AJ, Williams IH. 1997. *Chem. Commun.*, pp. 1271–72

265. Turner AJ, Moliner V, Williams IH. 1999. *Phys. Chem. Chem. Phys.* 1:1323–31

266. Moliner V, Williams IH. 2000. *Chem. Commun.*, pp.1843–44

267. Cunningham MA, Ho LL, Nguyen DT, Gillilan RE, Bash PA. 1997. *Biochemistry* 36:4800–16

268. Cunningham MA, Bash PA. 1999. *ACS Symp. Ser.* 721:384–400

269. Garcia-Viloca M, Gonzalez-Lafont A, Lluch JM. 2001. *J. Am. Chem. Soc.* 123:709–21

270. Han W-G, Tajkhorshid E, Suhai S. 1999. *J. Biomol. Struct. Dyn.* 16:1019–32

271. Harrison MJ, Burton NA, Hillier IH. 1997. *J. Am. Chem. Soc.* 119:12285–91

272. Ridder L, Mulholland AJ, Vervoort J, Rietjens IMCM. 1998. *J. Am. Chem. Soc.* 120:7641–42

273. Ridder L, Mulholland AJ, Rietjens IMCM, Vervoort J. 2000. *J. Am. Chem. Soc.* 122:8728–38

274. Ridder L, Palfey BA, Vervoort J, Rietjens IMCM. 2000. *FEBS Lett.* 478:197–201

275. Ridder L, Mulholland AJ, Rietjens IMCM, Vervoort J. 1999. *J. Mol. Graph. Model.* 17:163–75

276. Waszkowycz B, Hillier IH, Gensmantel N, Payling DW. 1991. *J. Chem. Soc. Perkin Trans. 2*, pp. 2025–32

277. Waszkowycz B, Hillier IH, Gensmantel N, Payling DW. 1991. *J. Chem. Soc. Perkin Trans. 2*, pp. 225–31

278. Schürer G, Lanig H, Clark T. 2000. *J. Phys. Chem. B* 104:1349–61

279. Hart JC, Burton NA, Hillier IH, Harrison MJ, Jewsbury P. 1997. *Chem. Commun.*, pp. 1431–32

280. Burton NA, Harrison MJ, Hart JC, Hillier IH, Sheppard DW. 1998. *Faraday Discuss.* 110:463–73

281. Moliner V, Andres J, Oliva M, Safont VS, Tapia O. 1999. *Theor. Chem. Acc.* 101:228–33

282. Antonczak S, Monard G, Ruiz-Lopez MF, Rivail J-L. 1998. *J. Am. Chem. Soc.* 120:8825–33

283. Antonczak S, Monard G, Lopez MR, Rivail J-L. 2000. *J. Mol. Model.* 6:527–38

Annual Review of Physical Chemistry
Volume 53, 2002

Contents

ERRATA
   An online log of corrections to *Annual Review of Physical Chemistry* chapters
   may be found at http://physchem.annualreviews.org/errata.shtml